Lumped parameters modelling of the EMAs' ball screw drive with special consideration to ball/grooves interactions to support model-based health monitoring

Lumped Parameters Modelling of the EMAs' Ball Screw Drive with Special Consideration to Ball/Grooves Interactions to Support Model-based Health Monitoring

Antonio Carlo Bertolino [1], Massimo Sorli, Giovanni Jacazio, Stefano Mauro
Department of Mechanical and Aerospace Engineering, Politecnico di Torino, 10129 Torino, Italy

Abstract

Building a high-fidelity model to identify a connection between a measurable signal variation and the onset and growth of a fault, which can then evolve in a failure, is a method to develop a prognostic and health management system. With this goal, this paper is focused on the development of a high-fidelity dynamic model of the ball screw component of flight control electro-mechanical actuators. This model can represent the roll/slip transition in the spheres/grooves contact points depending on dynamic operative conditions. It is suitable for various defects injection, such as friction increase, preload variation or mechanical backlash. The effect of such defects on the mechanical direct efficiency is investigated since it is a parameter which can be easily measured experimentally, and which may be a suitable candidate as health feature or as an indicator of faults onset and progression within the mechanism. This approach is intended to track the health status of the component and consequently avoid unexpected in-service failure, which may have a high cost, especially in the aerospace sector.

Keywords: Ball screw; Electro-mechanical actuator (EMA); Model-based health monitoring; High-fidelity physical model; Sensitivity analysis; Mechanism efficiency.

1. Introduction

In the last decades, in order to increase the efficiency and reduce pollution, a general trend in designing a "more electric aircraft" is ongoing [1–3]. To this purpose, a relevant step is the substitution of electro-hydraulic servo actuators (EHSAs) with electro-mechanical servo actuators (EMAs). This technology however is still struggling to spread in the aerospace sector [4–6] due to its too high jamming failure rate which makes it, in its standard configuration, not suitable for the actuation of primary flight controls. Several mechanical layouts have been proposed to reduce EMAs failure ratio [7–13], but they all lead to an increase of weight [14] or in additional maintenance requirements [15].

A different approach consists in continuously monitoring the health of the EMA through a prognostic and health management system (PHM) [16,17] to rapidly detect the onset of faults before they become critical and estimate the residual useful life. In order to acquire the knowledge required to develop a reliable PHM system, a deep analysis of the effects of possible fault entities and fault related parameters on the actuator performance under different operating conditions must be previously carried out [15,18]. This large amount of data can be obtained in a relatively cheap and fast way if a high-fidelity model of the EMA is developed. Previous studies have been made upon different components of the EMA architecture, such as the electric motor [19–22] and the electronic control unit (ECU) [23,24] as well as gears and bearings [25–27].

The aim of this work is to develop a lumped parameters high-fidelity dynamic model of the ball screw mechanism used for rotary to linear motion conversion in most EMAs. This component is the most prone to jamming issues according to the FMECA in [17], and its performance and duration depend on design and control parameters [28,29]. Due to the complexity of this mechanism, experimental analysis of the internal mechanical behaviour have been carried out only in very simplified scenarios [30,31] and therefore researchers tried to describe it with mathematical models. Hitherto, most of them considered static or quasi static conditions [32,33,42–45,34–41]. More detailed models, which describe the interaction between axial, torsional and lateral dynamics, are provided in [46–48], and [49,50] analyse the effect of screw compliance on the static load distribution. The dynamic models are mainly used in literature to perform only modal analyses and the system is described as a black box, which makes it not capable to describe the behaviour of single components and to capture the contact conditions at interface points. Besides, the more complex of these models, such as the FE ones, require a very high computational cost.

The model developed in this work introduces the possibility to consider the effects of the inertia properties of the ball screw system components, which can affect its overall efficiency during transients, especially when very low loads are applied. The model is developed in order to be used as a virtual test rig with the target to enable in the future easy injections of several kinds of defects and degradations to evaluate their effects on measurable signals of the ball screw itself or, in a future development, of a complete EMA. This approach, on

[1] Corresponding author. E-mail: antonio.bertolino@polito.it

this component, is not shared by any former author and allows to quickly carry out several simulations that can provide maps of measurable feature describing the system behaviour in presence of defects and degradations. Its results, if validated by experimental tests, will be useful to define prognostic algorithms for this component. Feng and Pan [51,52] tried to develop a similar data-driven procedure to diagnose a possible ball screw degradation, the preload level loss, linking it to the vibrational signal from accelerometers. Li et al. [53], considering a purely data-driven method, demonstrated that the ball screws are components on which it is possible to apply such an approach. Therefore, a detailed model would permit to obtain a better physical understanding and to study the system behaviour under normal and abnormal conditions. According to [15], to accurately reproduce the physic of ball screw jamming, it is crucial to create a precise model which can describe the wear and friction mechanism within the component, in the contact areas. This is also important because the friction increase has been identified as a jamming precursor [25]. For this reason, since the mechanical efficiency is directly related to the friction level, it has been identified as indicative of the health and wear status of the mechanism [25,54] and it can be used as a first health indicator. Therefore, it is analysed with regards to the variation of preload [51,55] and the friction increase due, for example, to the return channel jam [56] or an insufficient lubrication [25,57]. Many degradations are related to each other: for example, if the lubrication is insufficient the friction increases. It causes a temperature rise, which deteriorate the lubricant itself, but also creates more wear, since the lubricant film is thinner [58]. The wear of balls and grooves might create debris which enter into the lubricant and further contribute to the wear. All this process creates vibrations since the spheres now have to roll on worn irregular grooves: wear and vibrations entail the preload lessening and the increase of backlash, and so forth. All these faults create an exponential chain of faults progression and have an impact on the mechanical efficiency value, since they all imply power losses. At the same time backslash can arise because of the effect of wear [25,54,57], due to increased friction, or because of the loss of preload. In order to make possible a more complete analysis of the mechanism the proposed model includes the possibility of evaluating the effect of backslash; the results of diverse analyses of the effect of this parameter on the dynamic behaviour of the system are reported. Previous studies [59,60] showed that steady state mechanical efficiency is not affected by backlash.

The proposed model considers 5-dof and the motion of each component is described by its own d'Alambert's differential dynamic equilibrium equations, so that the inertia actions are taken into account. A preloaded double-nut single-cycle ball screw has been considered in this study, where the preload is obtained inserting a spacer between the two nuts: each sphere is considered to touch the grooves in two points only. The screw can only rotate while the nuts can only translate. Such a model is able to gather the time dependence of various signals, in particular the mechanical efficiency, and thus to obtain the dynamic performance as function of input and operating conditions. Moreover, on each sphere it is possible to discriminate between rolling and sliding conditions in both contact points with the screw and nut grooves. On these points, elastic deformations of the matching bodies are considered, and the normal and tangential forces can be computed. Finally, the proposed model considers the presence of a double-side backlash between the spheres and the grooves, and the presence of centrifugal effects. This model can describe the dynamics of each sphere and its interaction with the grooves dynamically as function of time and input values: therefore, it can be embedded into a more detailed model of the entire servo actuator as a ready-to-run subsystem. This allows to investigate the ball screw fault effects on the different EMA component dynamically, under real flight position demands and load time series. The model is fast to run, compared with the more detailed FE models, thus this allows numerous sensitivity analyses to be performed rapidly. This aspect is very important when creating a map of feature values versus fault levels, which is paramount to build a prognostic and health management system.

This paper first presents a short overview of a typical EMA architecture. Then it describes the high-fidelity non-linear dynamic model of the ball screw. Later, results obtained by this model are shown as well as the outcome of a sensitivity analysis on single and combined parameters on the mechanical direct efficiency. The influence of backlash and friction on the dynamic performance is investigated and, finally, the centrifugal force effect on normal and frictional contact forces and sliding conditions is analysed.

2. EMA Architecture

As already mentioned, one of the possible solutions to overcome the reliability issue is to adopt electro-mechanical actuators with a simple structure together with a PHM system. A typical architecture for such primary flight control EMAs is shown in Fig. 1.

Each equipped EMA has a dedicated Electronic Control Unit (ECU) which provides for the closed loop regulations and sends information about the EMA's status to the Flight Control Computer. The latter transmits the position set to the ECU of the different actuators in the aircraft. Usually, the position and velocity loops have digital controllers, while the current loop is fully analogic.

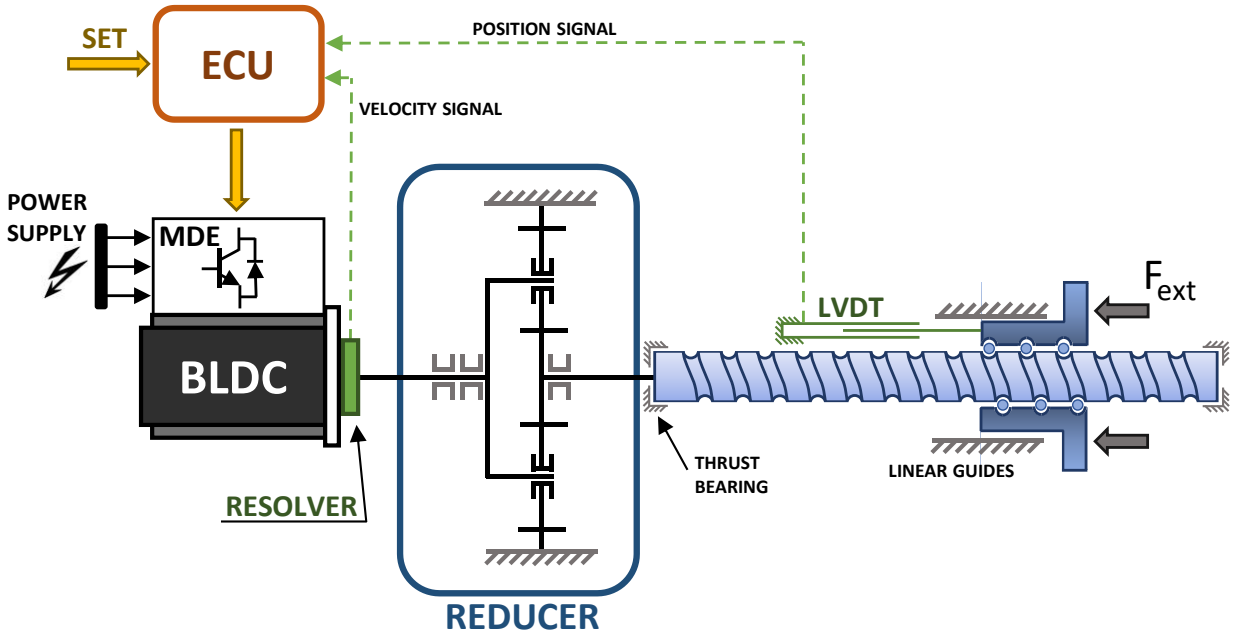

Fig. 1. Typical EMA architecture.

This kind of actuators are generally composed by an ECU, an electric motor with its electronics, a reducer, a ball or roller screw, a linear displacement sensor (typically an LVDT), a rotary speed sensor (e.g. a resolver) and other secondary components such as bearings, linear guides, brakes and a clutch to allow the motor and the mechanical part to be disconnected in case of emergency.

The ECU performs the speed and position control loops comparing the signals coming from the LVDT and the resolver, placed respectively on the translating part of the ball screw and on the high-speed shaft of the reducer. The resulting current command is the input to the Motor Drive Electronics (MDE), which operates the current control loop and generates the current command for the electric motor. The most popular solution is a brushless DC motor (BLDC) but sometimes it can be a switched reluctance motor as well. The output torque, through a reducer, is transmitted to the ball screw, which converts the rotating motion into linear motion. The external force is applied on the translating element from the aerodynamical loads acting on the control surface, directly attached to the EMA, together with the inertia actions of the surface and the kinematics, the friction effects and the loads exerted on the same surface by other actuators.

Generally, more than a single actuator is connected to the same control surface [61–63]. Therefore, undesired situations can occur, e.g. the force fighting condition, which happens when, in order to keep the surface steady, contrasting command, and then forces, are passed to the various involved actuators. Several strategies have been developed to avoid this situation [64].

If jam occurs, the entire transmission chain remains stuck in the last position reached before the failure and the EMA becomes useless and potentially dangerous for aircraft's governability. Typically, precursors of jamming are wear, backlash and friction increase, vibrations, hysteretic phenomena and noise.

Paper reference number	[59]	[60]	**Present paper**
Type of publication	Conference	Conference	Journal
Dynamics of screw, nuts and spheres	Yes	Yes	Yes
Double side contact model and backlash	Yes	Yes	Yes
Centrifugal force effect	No	No	Yes
Simulation results and information provided	Few	Few	Many
Combined parameter sensitivity analysis	No	No	Yes
Meaningful results at low external force	No	No	Yes
Simulation speed	Normal	Normal	Fast
Simulink implementation quality	Poor (frequent numerical instabilities)	Poor	Robust

Table 1. Summary of improvements with respect to previous articles.

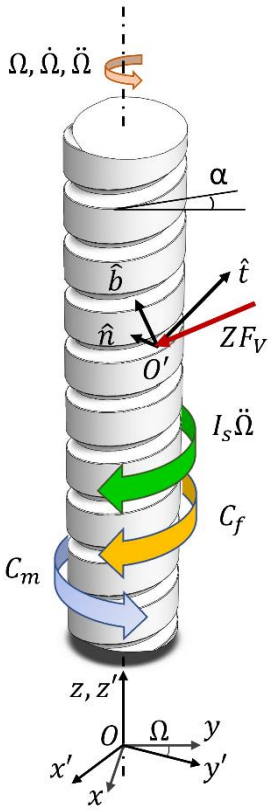

Fig. 2. Screw with reference systems and applied torques.

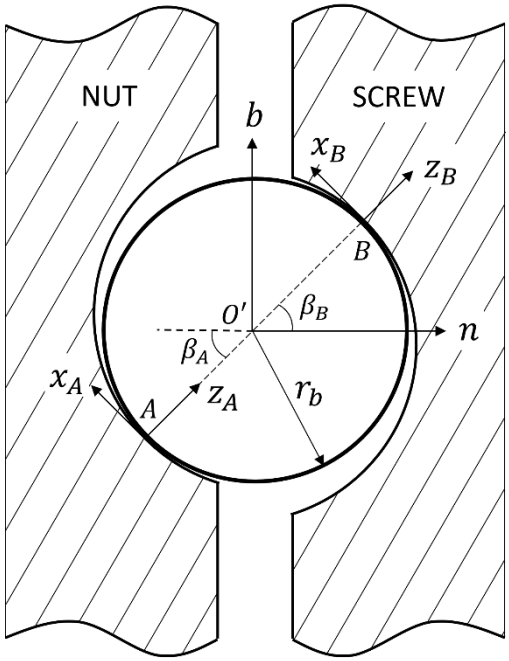

Fig. 3. Reference systems on the sphere.

3. Ball Screw Model

In this section a high-fidelity model of a ball screw drive is briefly presented. The basic equation framework of the model is the same of that described in [59,60], but a better implementation in the Simulink environment allows to avoid numeric instabilities and to slightly reduce the simulation time. A summary of the differences between the present formulation and those in [59,60] is reported in Table 1.

The model presented below is physics based. The motion of each component is described by its motion equations. Non-linear effects are taken into account in contact areas. The recirculation system is disregarded in this study, considering that when a sphere finishes the helical path it continues to roll starting again from the beginning of the path.

A preloaded double-nut ball screw was considered, where the screw can only rotate and the nuts are the translating parts. Compliance of joints is neglected. The following approach can still be applied if the nut rotates and the screw translates, with little modifications to the implementation.

3.1. Reference Systems

As Fig. 2 and Fig. 3 show, five reference systems have been adopted, according to [38,59,60]:

- $Oxyz$ is an inertial reference system, fixed in space with the z axis coincident with the screw axis;
- $Ox'y'z'$ has the z' axis parallel to z, and rotates with the screw shaft: the rotation angle is Ω;
- $O'tnb$ is the Frenet-Serret coordinate system, which describes the motion of one of the spheres. The origin is located in the considered sphere's centre, the t axis is tangent to the helical path, the n axis points towards the screw axis and b is the bi-normal axis;
- $x_i y_i z_i$ $(i = A_j, B_j)$ are two reference frames centred in the contact points of the sphere with the nut groove (A_j) and with the screw groove (B_j). For each one, the z_i axis is normal to the contact plane, and the y_i axis is parallel to the t axis.
- y_b is a mono-dimensional coordinate system along the rectified helical path. It represents the displacement of the centre of the sphere with regards to its initial position, where the origin is located.

where the subscripts i refers to the two contact points between the nut, the sphere and the screw, while the subscript j distinguishes the two nuts.

The angles $\beta_{A,j}$ and $\beta_{B,j}$ between the segment identified by contact points and the sphere's centre are the contact angles (Fig. 3); in this analysis, they are supposed to be constant and both equal to the most common

literature value of 45°. This means that the line which connects the two contact points identifies the direction along which forces are transmitted.
The rotational matrices between these reference frames are computed in [38].

3.2. Screw motion

Fig. 2 depicts the torques acting on the screw, which compose its dynamic equilibrium equation:

$$C_m - C_f - C_V - I_S\ddot{\Omega} = 0 \tag{1}$$

where C_m is the input torque from the motor, C_f is the friction torque and C_V is the torque obtained from the sum of all reaction forces from the spheres to the screw groove. It can be expressed as:

$$C_V = Z\sum_j \left[F_{V,j} + H_{B,j}\cos(\alpha')\right]\left[r_m - r_b\cos(\beta_B)\right] \tag{2}$$

where $H_{B,j}$ is the tangential friction force, along the t axis, from the spheres belonging to the j-th nut (§3.4) to the screw groove, while $F_{V,j}$ is the contact normal force projected in a direction tangent to the screw shaft and parallel to the xy plane.
Z is the actual number of spheres bearing load: usually this number is less than the total number of spheres due to possible manufacturing geometric errors and the presence of recirculating channels. According to literature [33,59,60,65], a good estimate can be:

$$Z = \lfloor 0.6Z_{tot} \rfloor = \left\lfloor 0.6\frac{2\pi r_m n_t}{2r_b\cos(\alpha)} \right\rfloor \tag{3}$$

The friction torque C_f is composed by the rolling friction torque $C_{rf,j}$ and the supports' frictional effects. The latter are represented through a Coulomb-Stribeck-viscous model [66] which allows lubricant effects to be considered and the simulation results to be more realistic. In the present work, this was neglected since the goal is to investigate only the mechanism's performance, without hindrances of supporting elements or different mounting conditions.

3.3. Nuts motion

The considered system has two nuts which are preloaded inserting a thickness between them, as in [67]. The preload force acts to separate the nuts, as illustrated in Fig. 4. The external force is shown applied on the nut's flange, but in the model it is considered equally distributed on both the nuts, basing on the assumption that all the spheres are equally loaded, without geometric errors and considering that the preload force is imposed as a constant force instead that as a spring, therefore it is not able to transmit the external force from one nut to the other. The matching forces between the spheres and the nut grooves are represented along the grooves: the total force $F_{Z,j}$ on each nut is derived from the projection and sum of all the contact forces from each sphere along the z axis. Since the analysed ball screw has a right-hand thread, to a positive rotation Ω of the screw corresponds a backwards displacement of the nut assembly with regards to the z axis.

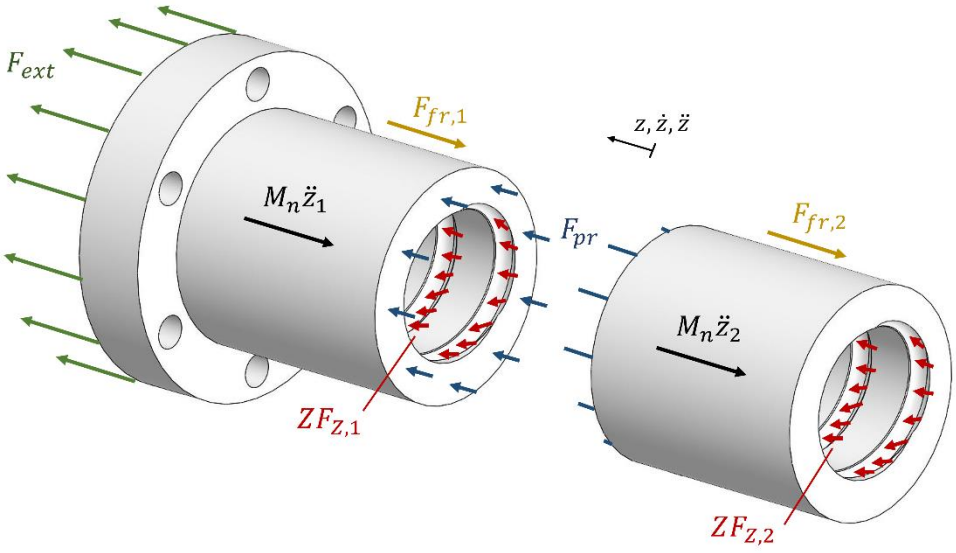

Fig. 4. Free body diagram of the nuts.

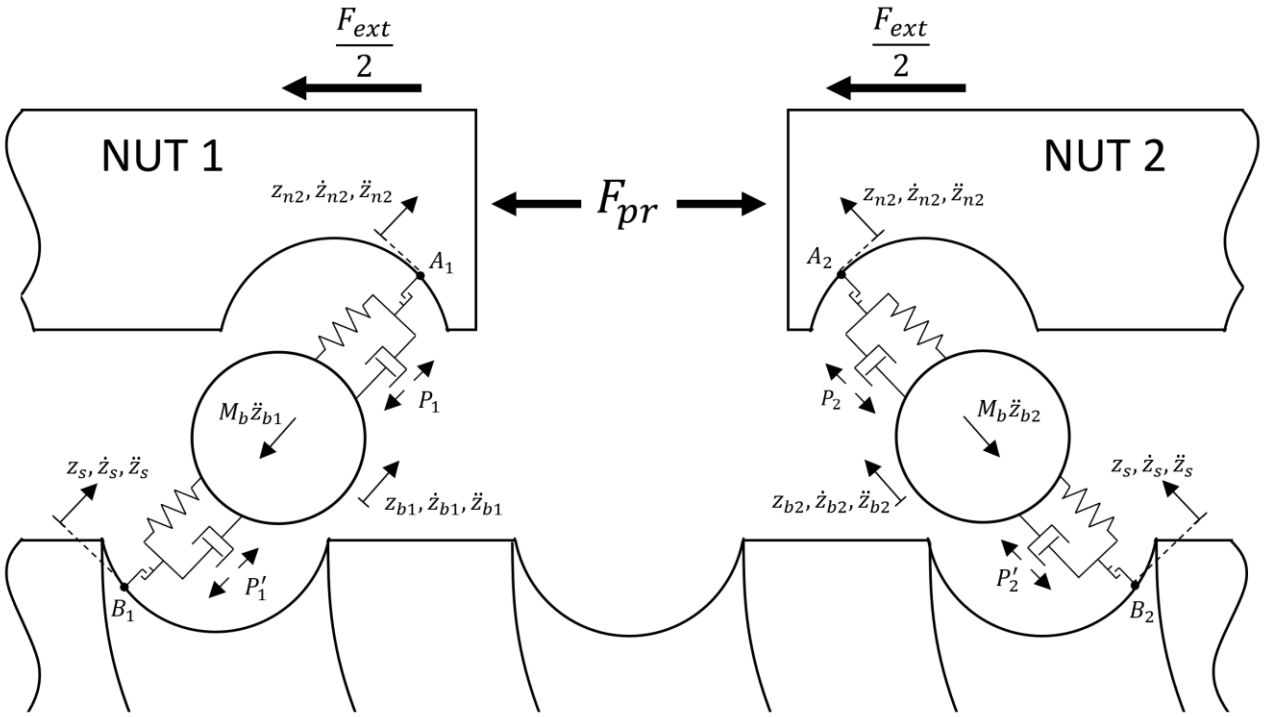

Fig. 5. Contact models between spheres, screw and nut. F_{ext} and F_{pr} are parallel to the z axis.

Each nut dynamic equilibrium equation is:

$$ZF_{Z,j} - F_{fr,j} + \frac{F_{ext}}{2} \pm F_{pr} - M_n\ddot{z}_j = 0 \tag{4}$$

As shown in Fig. 4, the preload sign is positive on the first nut ($j = 1$) and negative on the other one ($j = 2$). F_{fr} is the friction force applied on each nut and, as for the screw, it is composed by two parts: the friction given by the rolling/sliding spheres and the one due to the presence of linear guides, modelled by means of a Coulomb-Stribeck-viscous function as well. In the same way as for the screw, the latter has been disregarded in the present analysis to investigate only the ball screw itself. This means that idealized frictionless constraints have been adopted. The friction force can then be written as:

$$F_{fr,j} = H_{A,j}Zsin(\alpha'') \tag{5}$$

where $H_{A,j}$ is the tangential friction force between the sphere and the j-th nut groove, along the t axis (§3.4). The friction formulation adopted in Eqns. (1) and (4) is able to reproduce the stiction behaviour.

3.4. Spheres motion

Solving Eqns. (1) and (4) requires knowing the forces exchanged, through the spheres, in the contact regions, P_j and P_j'. The load is considered to be applied symmetrically with regards to the screw axis, therefore, neglecting geometric errors and the presence of radial loading, each sphere can be considered to bear the same fraction of the total load. Interactions between adjacent spheres are disregarded in this work. Thus, only one sphere is analysed and dynamically described, considering it as representative of the behaviour of all the others. In this paper only the linear dynamics along the y_i and z_i axes, the rotational dynamics around the x_i axis and centrifugal force are considered for each sphere. Gyroscopic effects, the rotational dynamics around y_i and z_i axes and the linear dynamics along the x_i axis are neglected. The subscript j will hence be omitted where possible for seek of clarity in notation.

The contacts have been modelled inserting spring and damper elements between the two impacting bodies, as shown in Fig. 5. The resulting system has five degrees of freedom: the screw, two spheres and two nuts. The motion is imposed from the screw and each sphere/nut sub-assembly moves linearly along the z_i axis, i.e. along the contact line. The model provides the possibility to insert a double sided backlash in each contact point, as shown in Fig. 5, according to the approach of [59,60,68,69]. Once the contact forces are calculated, they are used to solve Eqns. (1) and (4).

The equilibrium equation of each sphere along the z_i axis can be written as follow:

$$M_b\ddot{z}_{b,j} + P_j' - P_j = 0 \tag{6}$$

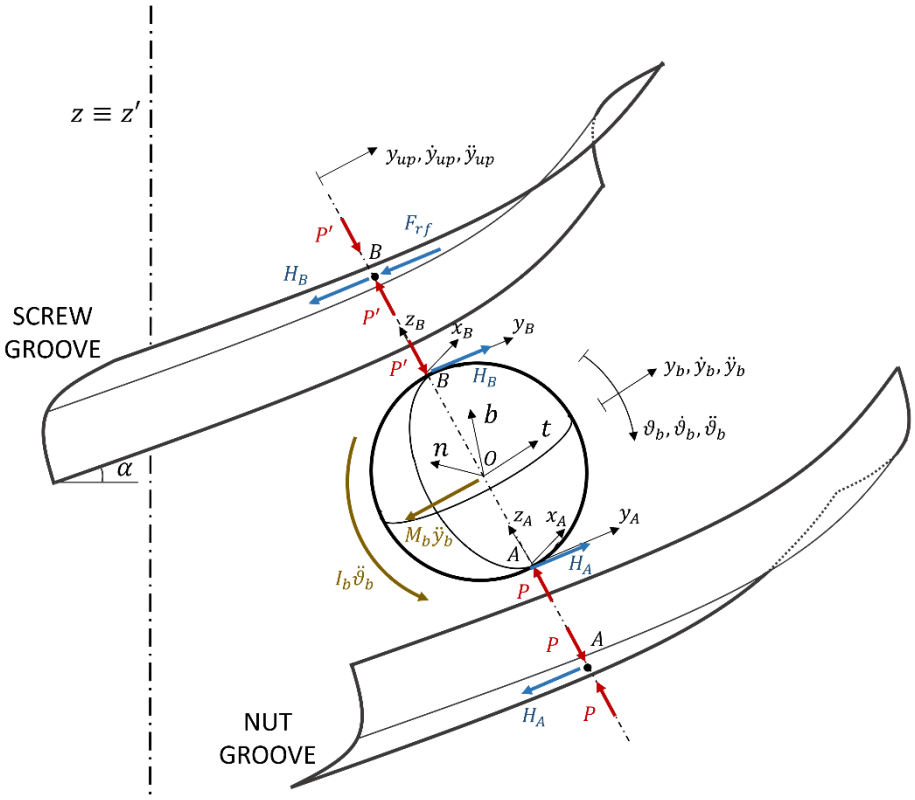

Fig. 6. Sphere's free body diagram.

$$P'_j = \left\{k\Delta z_{bs,j} + \not{f}\left[c\left(\dot{z}_{b,j} - \dot{z}_s\right), k\Delta z_{bs,j}\right]\right\}\left|H_{c,j}\right| \qquad (7)$$

$$\Delta z_{bs,j} = \left(z_{b,j} - z_s\right) - H_{c,j}\frac{b_{max}}{4}$$

$$P_j = \left\{k\Delta z_{nb,j} + \not{f}\left[c\left(\dot{z}_{n,j} - \dot{z}_{b,j}\right), k\Delta z_{nb,j}\right]\right\}\left|H_{c,j}\right| \qquad (8)$$

$$\Delta z_{nb,j} = \left(z_{n,j} - z_{b,j}\right) - H_{c,j}\frac{b_{max}}{4}$$

Since the contact angles are fixed, when the motion is reversed the spring-damper systems undergo tractive forces: therefore, when the contact forces are negative, it must be interpreted as if the contact angles instantaneously have changed from 45° to -45°. For example, in Fig. 5, one sphere bears the load with a positive contact angle while the other sphere with a negative one, thus also two contact forces are positive and the other ones are negative. In order to avoid discontinuities and spikes, as the impact speed grows, when the contact happens, the function $\not{f}$ and the coefficient $H_{c,j}$ have been introduced. When the contact forces are positive, i.e. $\beta_j = 45°$, $\not{f} = min$ and $H_{c,j} = 1$, while in the other case $\not{f} = max$ and $H_{c,j} = -1$. If backlash is considered, a third situation can occur, that is when the sphere does not have any active contact. This means that $\left|\Delta z_{bs,j}\right| = \left|\Delta z_{nb,j}\right| < b_{max}/4$ and therefore the coefficient $H_{c,j}$ is imposed equal to zero. When the backlash has to be neglected, it is sufficient to put $b_{max} = 0$.

The motion along the z_i axis, normal to the contact planes, is imposed by the displacement of the contact point B obtained from the screw rotation. Exploiting rotational matrices from [38], it is possible to derive it as:

$$z_s = -\frac{p}{2\pi}\Omega\cos(\alpha')\sin(\beta_B) \qquad (9)$$

The displacement of each nut $z_{n,j}$ on z_i axis can be linked with the axial translation z_j along the screw axis:

$$z_{n,j} = z_j\cos(\alpha'')\sin(\beta_A) \qquad (10)$$

The contact forces P_j and P'_j can be brought back to $Ox'y'z'$ reference frame in order to calculate, respectively, the reaction force on each nut, $F_{Z,j}$ in Eq. (4), and on the screw, $F_{V,j}$ in Eq. (2):

$$F_{V,j} = P'_j\sin(\alpha')\sin(\beta_B) \qquad (11)$$

$$F_{Z,j} = -P_j\cos(\alpha'')\sin(\beta_A) \qquad (12)$$

	Description	Value	Units
Geometrical parameters			
I_s	Screw moment of inertia around z axis	$9.8 \cdot 10^{-4}$	kg m^2
n_t	Loaded turns number	3	
M_n	Nut mass	1.3	kg
p	Screw lead	20	mm
r_b	Ball radius	3	mm
r_m	Screw pitch circle radius	20	mm
Z_{tot}	Total number of spheres	63	
α	Nominal helix angle	9.043	deg
α'	Inner helix angle	10.095	deg
α''	Outer helix angle	8.188	deg
β	Contact angle	45	deg
Performance parameters			
F_{max}	Critical stall load	43.43	kN
k_{ax}	Axial stiffness	1.27	kN/μm
Ω_{cr}	Critical screw angular speed	2400	rpm
Nominal conditions			
$b_{max,nom}$	Backlash in nominal conditions	0	μm
$F_{ext,nom}$	External nominal force	21.72	kN
$F_{pr,nom}$	Nominal preload	7.67	kN

Table 2. Screw parameters and assumed nominal conditions.

For the sphere's rolling motion, an approximation was made: it was considered unidimensional along the helical path as if it was rectified: each sphere can thus rotate only around the x_i axis and the displacement is always parallel to $y_i \equiv t$ axis. The motion occurs in the $y_i z_i$ plane and the nut groove is considered fixed because the nuts does not rotate and because the coordinate system y_b, used to determine the displacement of the sphere, is fixed with the nut. In both contact point there can be either sliding or rolling depending on the operating conditions.

As for the dynamics in the z_i axis, the rolling motion is governed by the screw's rotation. The displacement of the contact point B along y_i, considered integral with the screw groove, is known from Eq. (1) and can be expressed as:

$$y_{up} = \frac{p\Omega}{2\pi \sin(\alpha')} \tag{13}$$

Neglecting gyroscopic effects, simple dynamic equation can be easily derived from Fig. 6 for both the translational and rotational motion in the $x_i y_i$ plane. The forces H_A and H_B are tangential contact forces which arise during rolling. They act both on the sphere and on the grooves, therefore they contribute to the reaction and friction forces and torques on the nuts and the screw. H_A and H_B are obtained adopting the continuous differentiable formulation proposed by Makkar et al. [70] which links the friction coefficient with the contact slip speed.

The equivalent effect of rolling friction on the considered sphere has been moved as a tangential force on the screw, F_{rf}, parallel to y_i. This force, properly projected by means of rotational matrices, becomes the component C_{rf} of the friction torque C_f in Eq. (1). Then, F_{rf} has been expressed, according to [59,60], slightly adapting the formulation in [71]:

$$C_{rf} = F_{rf} Z \cos(\alpha') \left[r_m - r_b \cos(\beta_B)\right] \tag{14}$$

$$F_{rf} = \sum_j \left(P_j f_{v,j} + P_j' f_{v,j}'\right) \tag{15}$$

$$f_{v,j} = f_{v0,j} + f_{v1} \dot{\vartheta}_{b,j}^2 \tag{16}$$

$$f_{v0,j} = \frac{P_j^{0.26} k_{gc}}{r_b} k_{rf} \tag{17}$$

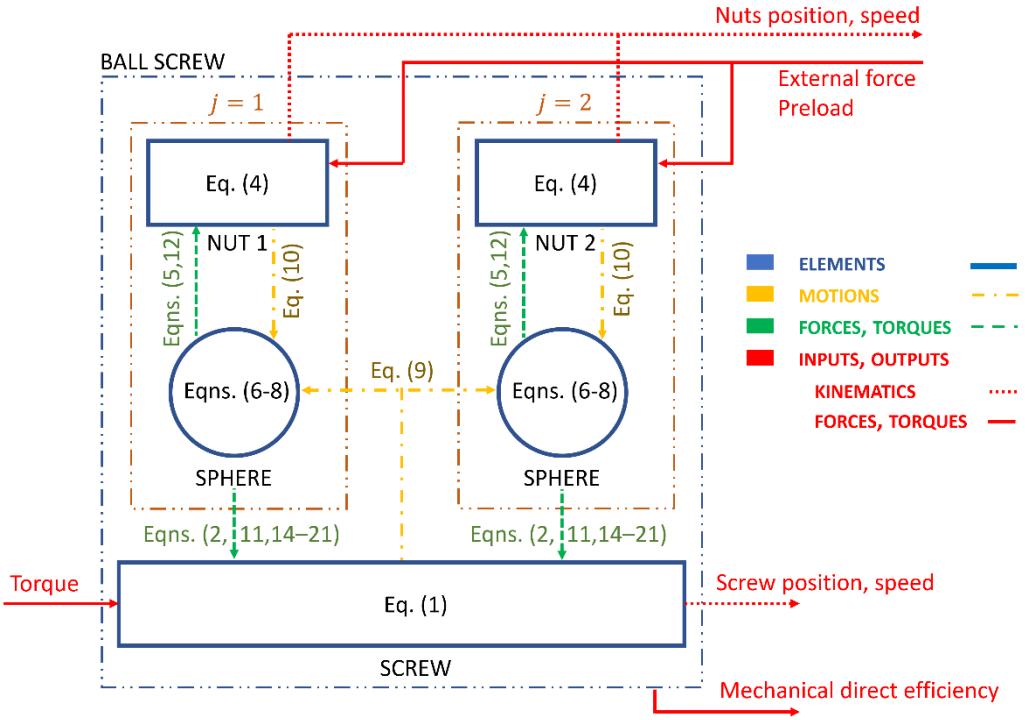

Fig. 7. Graphical model implementation.

$$f'_{v,j} = f'_{v0,j} + f_{v1}\dot{\vartheta}^2_{b,j} \tag{18}$$

$$f'_{v0,j} = \frac{{P'_j}^{0.26} k_{gc}}{r_b} k_{rf} \tag{19}$$

Since the rolling friction depends on the contact loads and on the sphere's rolling angular speed, the rolling friction coefficient u is not constant and it can be rewritten considering Eqns. (15) – (19) as:

$$u_j = k_{gc} k_{rf} P_j^{0.26} + f_{v1} r_b \dot{\vartheta}^2_{b,j} \tag{20}$$

$$u'_j = k_{gc} k_{rf} {P'_j}^{0.26} + f_{v1} r_b \dot{\vartheta}^2_{b,j} \tag{21}$$

where k_{gc} is the coefficient of load dependence and f_{v1} of speed dependence of the rolling friction k_{rf} is a parameter which allows to modify the friction effect on the system and will be used in the sensitivity analysis. It is well known that for low loads the rolling friction coefficient is little dependent on the load and the relationship $u = kP^{0.2}$ is typically used, while for higher loads the Gerstener-Coriolis expression $u = k\sqrt[3]{P}$ is applicable [72]. Then, for the purpose of this analysis, an average dependence of the rolling friction coefficient with the load has been assumed and the normal force exponent has been set on 0.26. The contribution to the rolling friction coefficient given by the angular rolling speed $\dot{\vartheta}_b$ is squared because of the local kinetic energy dissipation due to micro-impacts of the material of the sphere when it enters into the contact area.
Finally, the direct efficiency has been calculated as power ratio, cleaned of the inertia effects in order to evaluate it also in dynamic conditions and transients:

$$\eta = \frac{[F_{ext} + M_n(\ddot{z}_1 + \ddot{z}_2)]\dot{z}}{(C_m - I_s\ddot{\Omega})} \tag{22}$$

A graphical implementation of the model is shown in Fig. 7, where the inputs are the driving torque, the external force and the preload and the outputs are the screw angular speed and rotation and the nuts speed and displacement.

4 Analysis and Discussion

The above presented model was used to evaluate performances of a double-nut single-cycled preloaded ball screw with the characteristic dimensions listed in Table 2. Nominal values are listed as well: they have been assumed by the authors as reference operating conditions with regards to which sensitivity analysis was performed. The nominal external force is half the critical axial load and the nominal preload has been identified following the prescription of the ISO 3408-4:2006 standard [73]:

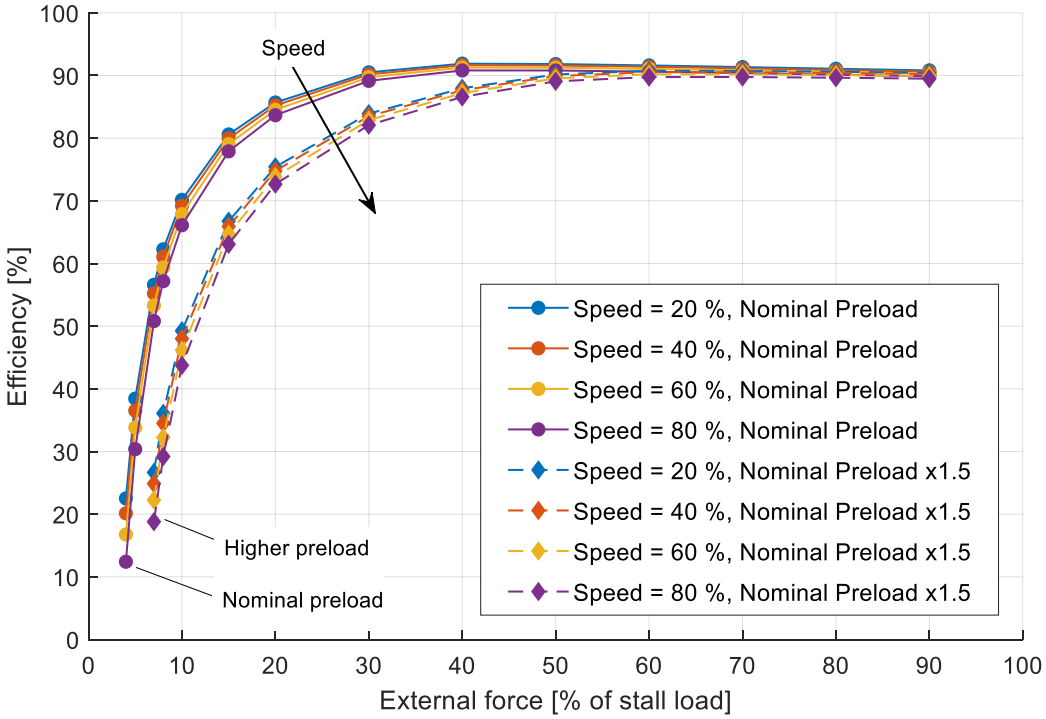

Fig. 8. Sensitivity analysis on the mechanical direct efficiency with regards to the external force, screw speed and preload, with $k_{rf} = 1$.

$$F_{pr,nom} = \frac{F_{ext,nom}}{2^{3/2}} = \frac{0.5F_{max}}{2^{3/2}} \tag{23}$$

In this section a sensitivity analysis of single parameter variations on the mechanical direct efficiency is presented. Furthermore, the results of different analyses on the combined effect of several parameters on the mechanical direct efficiency is described. Later, the effect of friction and backlash in dynamic conditions are investigated. Finally, the effect of the centrifugal force on the normal and tangential friction forces and on the rolling/slipping condition of the sphere in the contact points is shown. All the results have been obtained simulating the model with the fixed step solver ode14x with first extrapolation order. This choice helps to obtain more physically meaningful results and to overcome the problems which can arise due to the presence of small masses, i.e. the spheres, connected with high contact stiffnesses. This condition can lead to significant slow down of simulations in transient conditions when using variable step solvers. Furthermore, the choice to use the ode14x solver comes from the fact that this model will be embedded in a more complex model of an EMA, whose motor is controlled through a PWM signal. This module requires a fixed step solver in order to simulate, due to the presence of numerous instantaneous steps.

4.1. Sensitivity analysis

The mechanical direct efficiency versus the external force is shown in Fig. 8, varying the preload and the screw speed, expressed as a percentage of the critical speed Ω_{cr} for transverse vibration. This value is defined as the speed at which the system will reach its first critical frequency and therefore it may resonate and eventually become unable to operate. According to ball screw manufacturer catalogues, an estimation of its value in rpm can be obtained by the following formula:

$$\dot{\Omega}_{cr} = 0.8\frac{60}{2\pi}\sqrt{\frac{cIE}{Wl^3}} \tag{24}$$

where E is the Young modulus of the screw, W is the screw weight, l is the distance between the constraints and I is the section moment of inertia, calculated considering the root diameter of the screw instead of the outside diameter in order to maintain a safety factor. The coefficient c depends on supports types: in this study it has been considered equal to 8, corresponding to a fixed-free configuration. An additional safety coefficient of 0.8 multiplies the result. The obtained critical speed is reported in Table 2.

From Eq. (22) it can be seen that when the external force tends to zero the mechanical direct efficiency does the same. When the external force increases, the mechanical direct efficiency does not grow indefinitely, but shows a maximum. This is due to the load dependent rolling friction in Eqns. (20,21) which scales with a power of the normal load on the spheres. For high values of external load, the trend is almost linearly

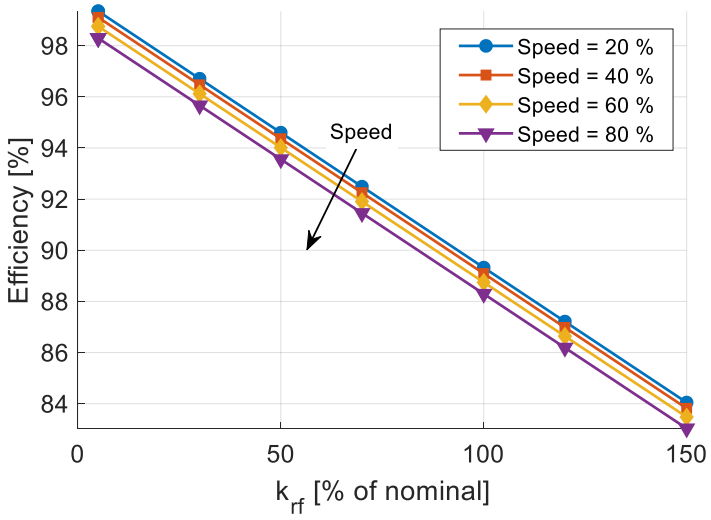

Fig. 9. Sensitivity analysis on the mechanical direct efficiency with regards to the friction parameter, varying the screw speed, with nominal preload and external force.

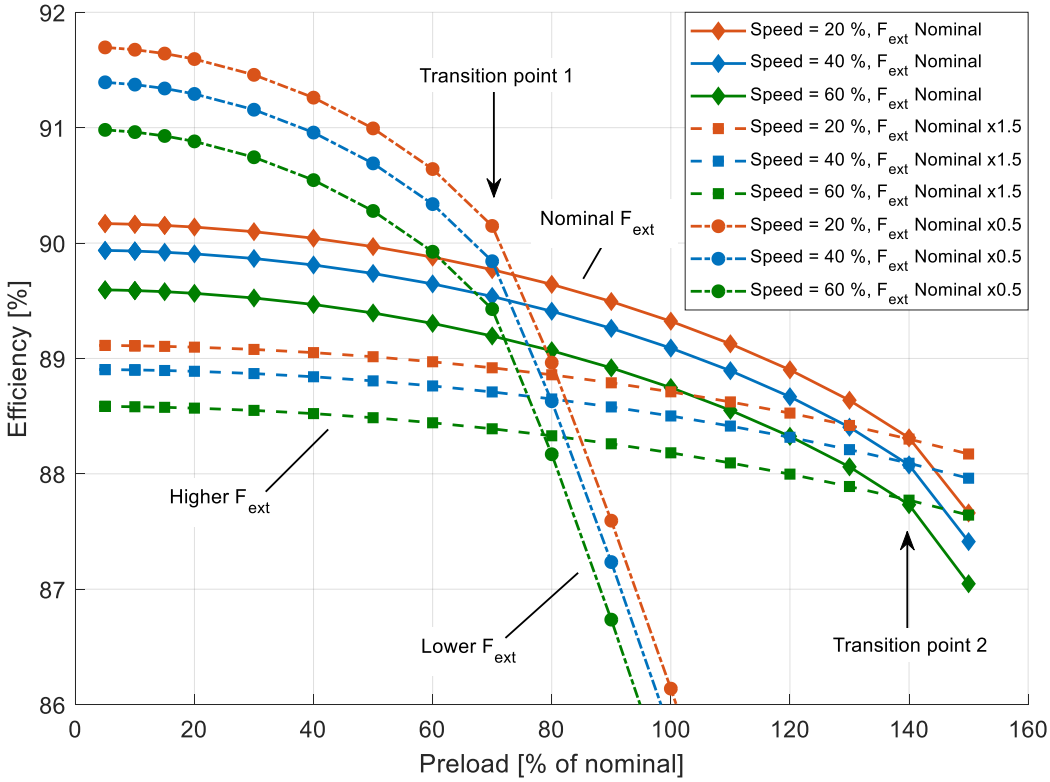

Fig. 10. Sensitivity analysis on the mechanical direct efficiency with regards to the preload, varying the screw speed, with $k_{rf} = 1$.

decreasing. The direct efficiency depends upon the spheres' speed as well, which is related to the screw angular speed by known cinematic equations [34]. Since the rolling friction depends on the square of the angular speed, in Fig. 8 several parallel curves show the reduction of the direct efficiency with an increase of the screw speed. Another important parameter is the preload, which causes an offset in the load on the spheres. Therefore, with the same external force, the load carried by each sphere is higher and thus the direct efficiency is lower. Even with a different preload, the trend at high external forces is nearly linear, and converges to the same values. The point of maximum mechanical direct efficiency moves at higher external force values for increasing preloads. Highlight on the combined effect of external force and preload are given in the following section.

Fig. 9 depicts the dependence of the mechanical direct efficiency on the k_{rf} parameter of Eqns. (15-19). This parameter is a multiplicative factor to increase the load dependent component of the rolling friction. The mechanical direct efficiency is influenced linearly by the friction and, from Eq. (17,19) it depends linearly from k_{rf}: therefore, the trend is linear and it drops as the friction increase. The effect of the speed is the same as above. The friction increase can be considered as a representative effect of the grooves wear or of the

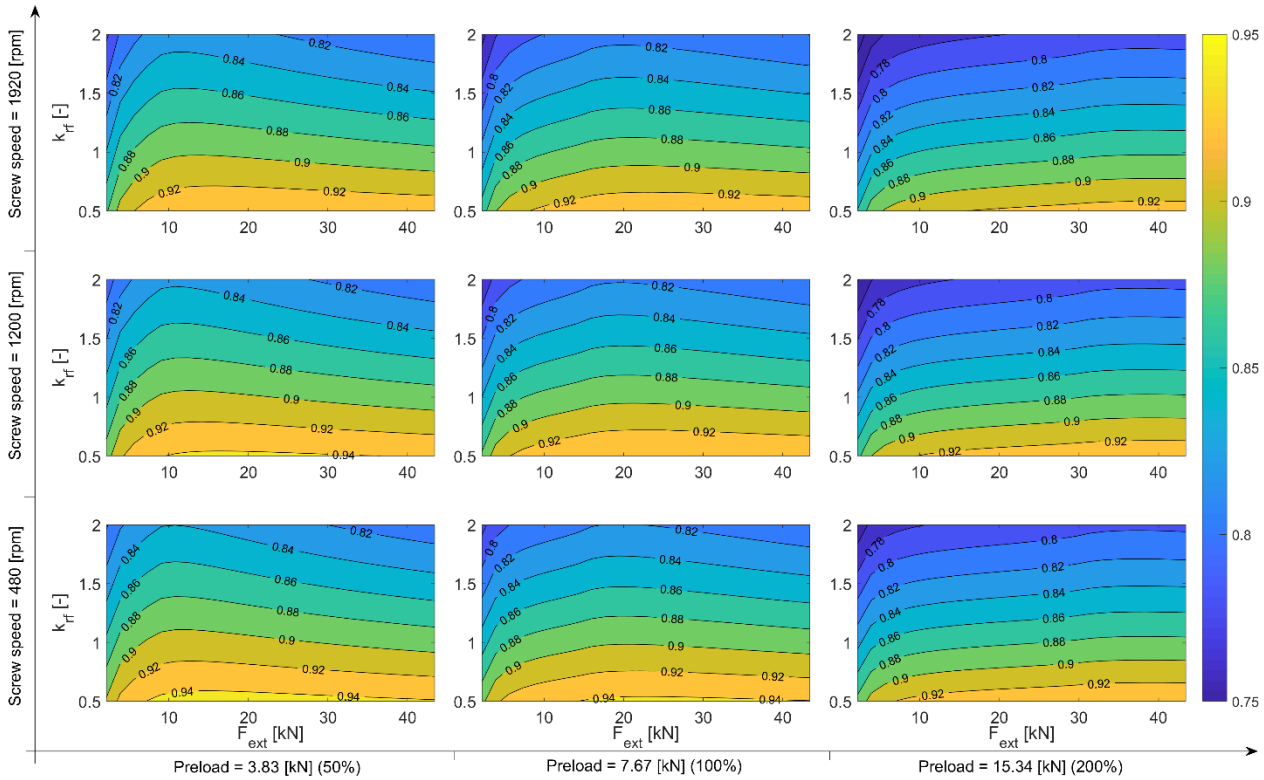

Fig. 11. Four-dimensional map of mechanical direct efficiency, with regards to the external force, the preload, the friction coefficient and the screw angular speed.

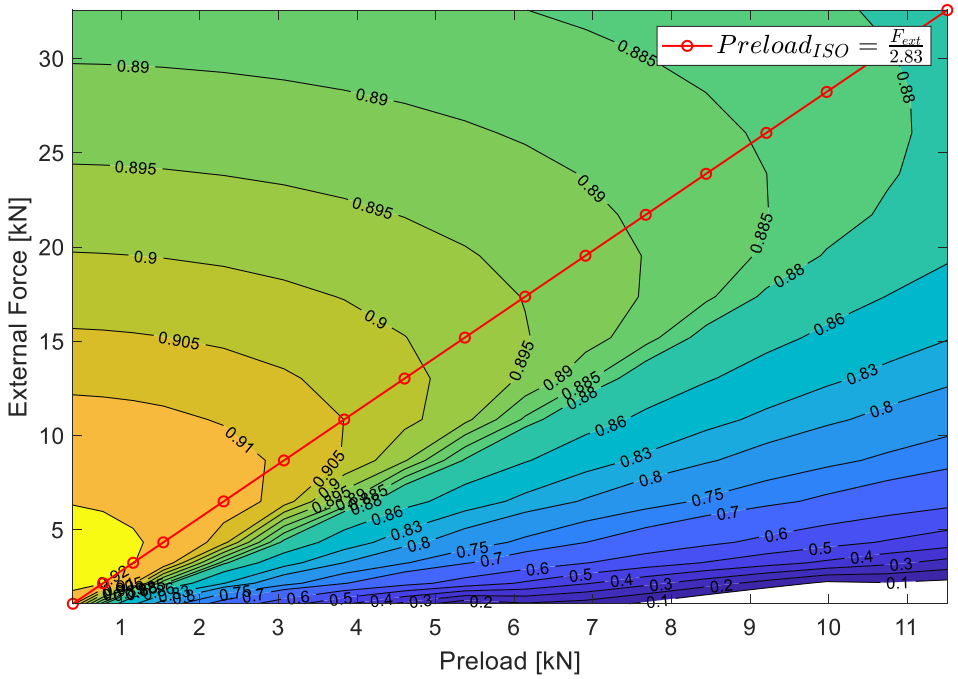

Fig. 12. Combined effect of external force and preload on the mechanical direct efficiency, with $k_{rf} = 1$ and $\Omega = \Omega_{cr}/2$.

degradation of the lubricant.

The dependence of the mechanical direct efficiency on the preload force is depicted in Fig. 10. The speed influence shows the same trend as for the previous parameters. There exist three family of curves with different slopes: each of them is relative to a different value of external load. Considering that the friction depends on the power 0.26 of the contact forces, the external load determines the operating point around which the systems moves varying the preload. For high values of external force, the operating point is in the flat zone of the power curve, thus the direct efficiency decreases more slowly with the preload. Vice versa, for low external forces, the direct efficiency is higher for low preloads, but it drops quicker as the preload increases because the

operating point lays in the slant part of the power curve. Looking at Fig. 5, it can be noted that, when the preload value approaches $F_{ext}/2$, the spheres of the nut which has the preload force in the opposite direction with respect to the external force, are almost unloaded. Hence, all the load is carried by only one nut. This point is indicated in Fig. 10 as "transition point". Its location is different for sundry preload values: obviously higher external forces leads to greater transition point preload values. Beyond these points the behaviour is approximately linear, due to the fact that the spheres which are highly loaded are in the flat part of the friction-contact force curve, while the others, which are roughly unloaded, are in the steep region of that curve, which is nearly linear as well. Between them, the influence of the most loaded spheres on the total friction prevails.

4.2. Combined parameters effect

Fig. 11 reports the results of a multivariate sensitivity analysis on the mechanical direct efficiency, with respect to the external force, the preload, the speed and the rolling friction parameter. Three different speeds have been considered: 20%, 50% and 80% of the critical speed. The rolling friction parameter factor k_{rf} was considered continuously in the range $[0.5, 2]$ and its influence is linear. The external force was varied throughout its full range $[0, F_{max}]$, whereas, for the preload, three values have been taken into account: 50%, 100% and 200% of the nominal preload specified in Table 2. For low preload values, given a k_{rf} value, the maximum of the direct efficiency occurs for low values of the external force. Its location moves at higher external forces for higher preloads. The presence of the peak of direct efficiency is even more pronounced the higher is the k_{rf} factor. It can be noted that the maximum takes place roughly at an external force value which is near $2^{3/2} = 2.83$ times greater than the considered preload, which is in accordance with Eq. (23) and ISO standards [73]. The exponent $3/2$ comes from the Hertz theory for elastic contacts: indeed $2^{3/2}F_{pr}$ is the external force value at which one contact side becomes inactive, while, below this value, both contacts are active and no shock occurs when a contact becomes active again.

The complex relationship between the external load and the preload can be better visualized fixing k_{rf} to the nominal unitary value and the speed to an arbitrary value, equal in this case to $40\%\,\Omega_{cr}$, and plotting a bidimensional map of the direct efficiency with respect to the preload and external force, as in Fig. 12. From this picture, it is clear that, for a given external force, the ISO standard prescribes a preload value such that in nominal condition it would lead to have approximately the maximum possible direct efficiency. It is also clear that if the system meets different operating conditions the direct efficiency will be lower, according to Fig. 12. It is preferable to have external loads higher than the nominal one since it would cause a minor direct efficiency reduction, while the region below the straight line is a low efficiency area because the direct efficiency can drop to very low values. Actually, for flight control EMAs, the ball screw is usually designed to resist to the maximum possible load, which is in general very high since it could be due to wind gusts during flights. However, in the majority of its operating life, the actuator works with lower loads, that means in this low efficiency region. Nevertheless, again from Fig. 12, it can be noted that, considering the same external load, a higher direct efficiency can be obtained diminishing the preload. The optimal working point can thus be varied from the design working point, acting on the preload. On the contrary, a decrease of the preload, thought it would lead to higher direct efficiency in steady-state conditions, would cause dynamic performances reduction, such as diminution of dynamic stiffness and the insurgence of backlash, which are investigated in the next paragraph. Finally, it is evident how different parameters value can produce the same direct efficiency, therefore, alone, it is not sufficient to describe the health status of a ball screw component.

4.3. Dynamic effects of friction, backlash and centrifugal force in the contact areas

So far, all the performance evaluations have been made in steady-state conditions, calculating the direct efficiency at several constant speeds. In these conditions, the backlash doesn't affect the mechanical direct efficiency since the displacement is always in the same direction and thus the backlash gap is always closed [59,60]. To highlight the effect of the backlash, the ball screw model was inserted in a closed loop position control system, and a sinusoidal position command was imposed to the controller, with different backlash sizes and without external force and preload (Fig. 13). It can be noted that, the more the backlash increases, the more the nuts trajectory distances from the set command. The effect of friction is visible as well: if the friction wasn't present, at the first velocity inversion of the sinusoid, the nut assembly would continue straight, detaching from the rear backlash limit and crossing the command dashed line until it would hit against the front backlash limit. Instead, as the command approaches the velocity inversion point, the friction acts on the nut assembly and stops it earlier than the set position. Looking at the right plot of Fig. 13, this behaviour is clearer if the speed of the nut assembly is analysed: it drops to zero until the nuts engage again with the screw. Fig. 14 emphasizes the backlash effect representing the nuts position versus the screw equivalent linear

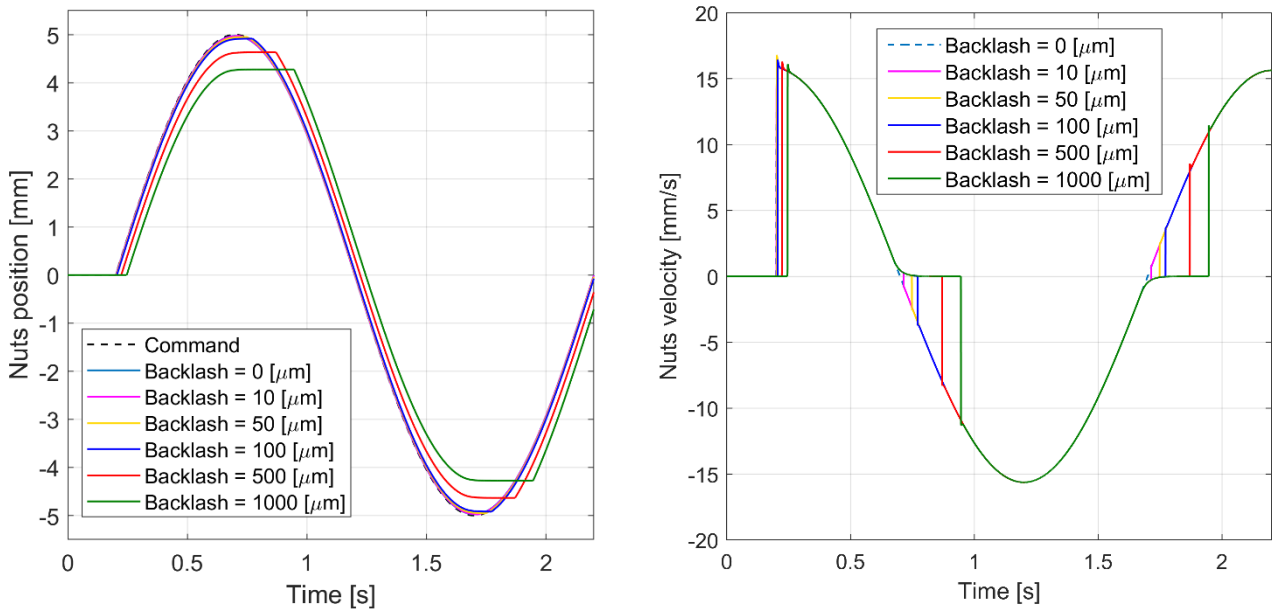

Fig. 13. Effect of friction and backlash on a sinusoidal nut displacement command, with no preload, no external force and $k_{rf} = 1$. On the left, the nuts displacement; on the right, the nuts velocity.

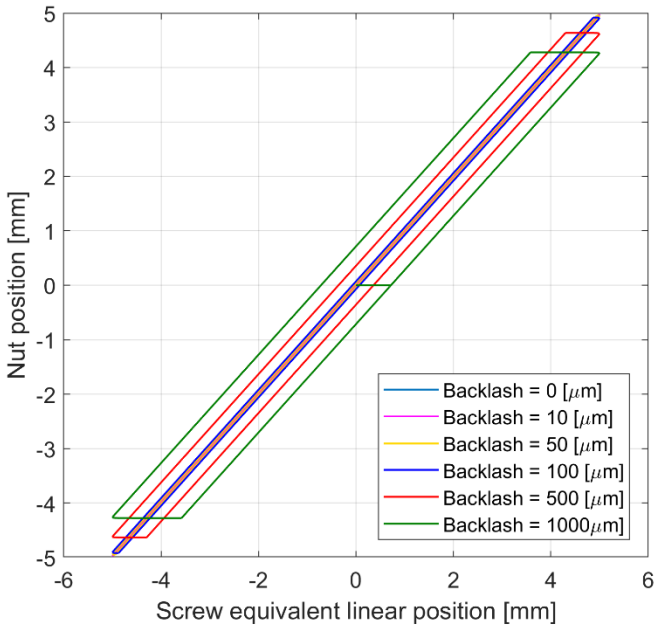

Fig. 14. Effect of friction and backlash on the hysteresis loop obtained by a sinusoidal nut displacement command, with no preload, no external force and $k_{rf} = 1$. On the left, the nuts displacement; on the right, the nuts velocity.

position. These hysteresis loops grow as the backlash increases. In this representation, the friction effect is not present, because it can influence only the hysteresis loop of the nut position versus the imposed command.
When external force and preload are applied in presence of backlash, different conditions can occur on the spheres of the two nuts, as depicted in Fig. 15. Six situations are represented, as well as the contact line orientation. The entity of load on each sphere is qualitatively indicated with SL (small load), NL (no load), HL (high load). If only the external force is applied (Fig. 15a and Fig. 15b) both spheres bear the same load, in the same direction. If also preload is present, the load on each sphere depends upon the ratio between the preload and the external force. If the preload is larger than the external force (Fig. 15c), the two spheres are loaded in opposite direction but the one on which the preload and external force sum up is more charged. If the preload is almost equal to the external force (Fig. 15d), only one sphere bears all the load, while the other is nearly unloaded. This is the situation described in Fig. 10 for the transition points in the direct efficiency curves. If the preload is smaller than the external force, as in Fig. 15e, both the spheres are loaded in the same direction, determined by the external force itself, and the one on which the preload and external force sum up is more

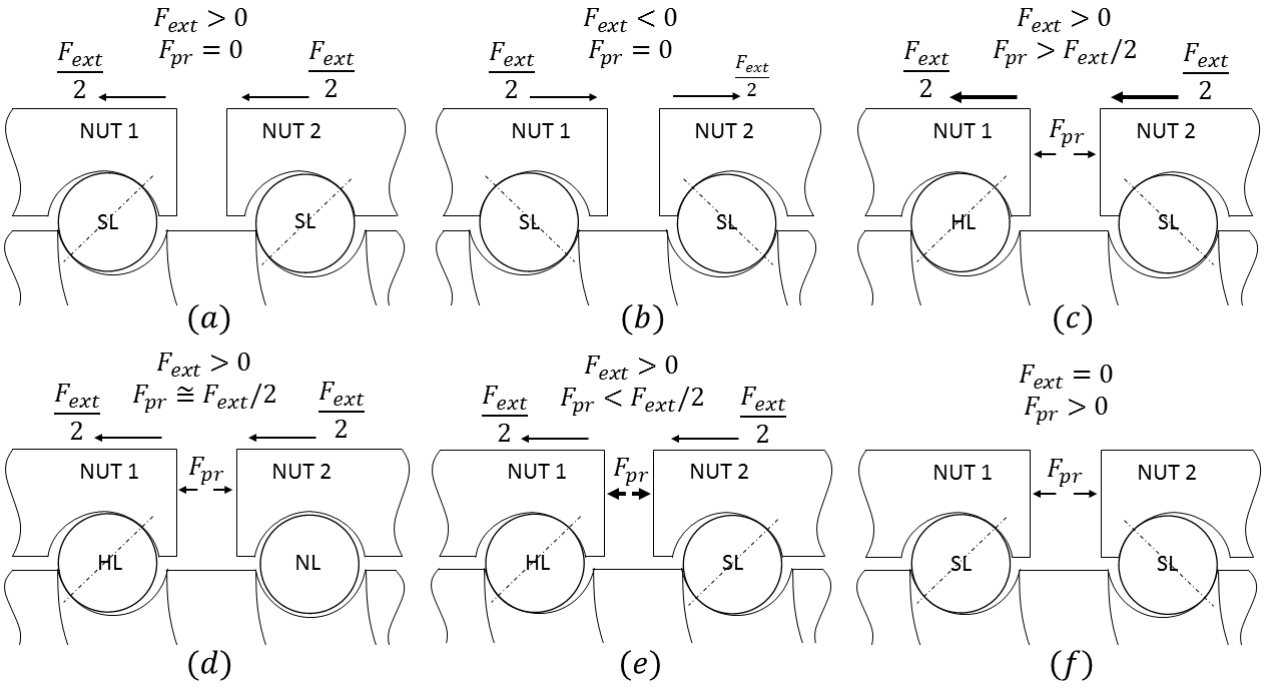

Fig. 15. Various loading conditions of the spheres of the two nuts in presence of backlash, depending on the external force and preload (SL: small load, NL: almost no load, HL: high load).

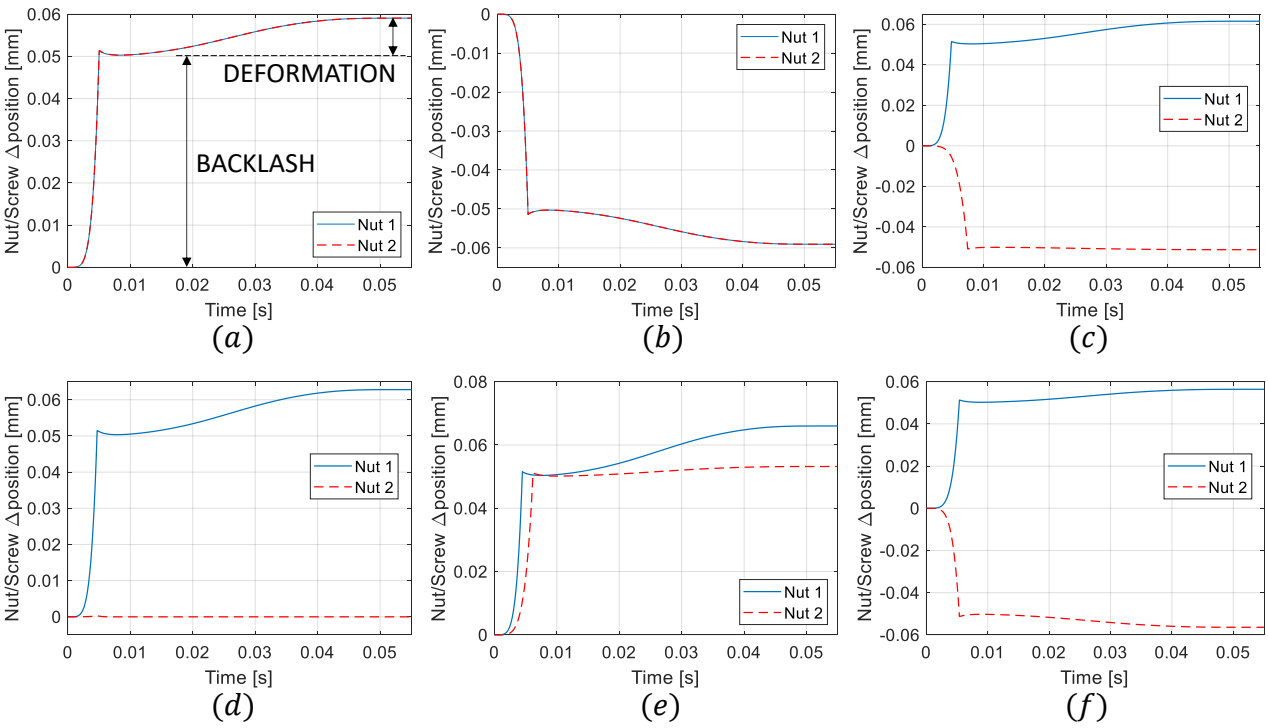

Fig. 16. Contact deformations calculated applying constant preload and external force according to loading condition of Fig. 15, in presence of backlash.

loaded. Finally, if only preload is present, both spheres are subjected to the same force and the contact lines have opposite inclination.

To verify that the model is capable to get this behaviour, constant preload and external force were applied, with a sigmoid function to avoid numeric instabilities, according to loading condition from Fig. 15. Deformation due to the contact forces on the spheres of each nuts are plotted in Fig. 16. These simulations were carried out setting the external force, the preload and the friction coefficient to their nominal value and imposing a backlash size on each nut of 0.1 mm. This means that, plotting the difference in linear position between the nuts and the screw, this can vary between $-0.05\,mm$ and $+0.05\,mm$. Further position discrepancies are due to elastic deformation in the contact points between spheres and grooves, as shown in Fig. 16a. The contact forces reflect the expected behaviour: e.g. in Fig. 16c the sphere of nut 2 is loaded in the

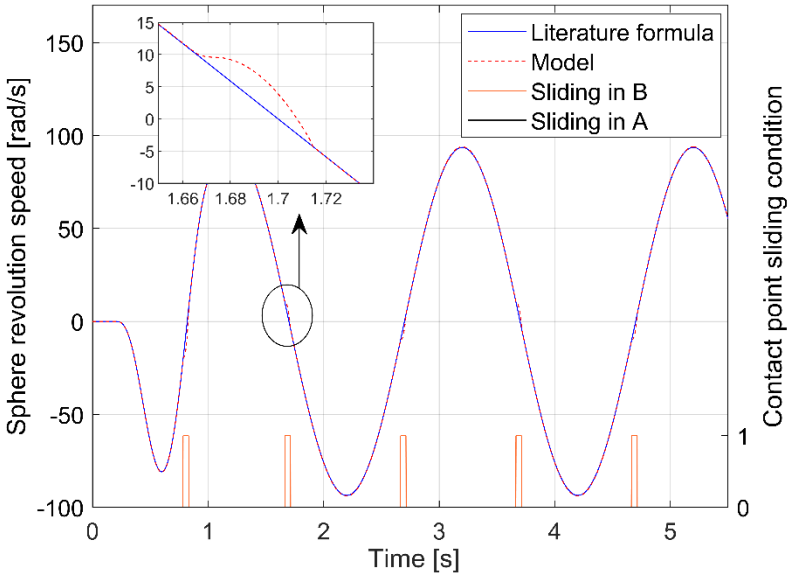

Fig. 17. Comparison between the revolution speed of one sphere obtained from the model with the result of the literature formula.

opposite direction with respect to the other, because the difference of position between the nut 2 and the screw is negative, and the elastic deformation are minor because it is less loaded. In Fig. 16e, the sphere of nut 2 is almost unloaded and therefore the nut 2 does not move, being in equilibrium between all the acting forces. In every situation, the position difference reaches first suddenly $\pm 0.05\ mm$, i.e. the backlash gaps close, and then elastic deformations take place.

The model capability to take into account backlash is important to be able to model more kinds of faults: the backlash increase can be representative of the grooves wear and can produce vibrations of the mechanism. Its effect is visible, given a known motion of the screw, on the position and speed signal of the nuts, which are measurable with generally available sensors. The analysis of these signals can be useful to understand the global wear level of the ball screw. Futhermore, its effect depends on the preload, which can be varied to represent a preload lessening which can happen during the operative life of a ball screw [51,74,75].

The present model allows to obtain the normal and tangential contact forces in both the contact points of each sphere, depending on their dynamic condition with regards to the grooves: the spheres have the rotational and translational different degrees of freedom in such a way they can either roll or slide in both the contact points. The contact forces could be used to assess the contact stresses, knowing the geometric parameters of the grooves and the spheres, and hence to perform fatigue analysis and to estimate the operative life. The contact forces are influenced by the centrifugal force, which has the effect to push the spheres towards the nut groove, increasing the contact force in the contact point A and decreasing that in the contact point B. This effect depends on the revolution speed of the sphere around the screw axis: the more it is high the more the centrifugal force is significative. Neglecting the gyroscopic effects and imposing both the contact angles equal to 45°, it can be expressed, according to [34,37], as:

$$\omega_{rev} = \frac{1}{2}\dot{\Omega}\left(1 - \frac{r_b}{r_m}\cos(\beta)\right) \tag{25}$$

The revolution speed obtained from the model matches the result of Eq. (25). Fig. 17 shows the comparison between the two curves, when to the ball screw is given a sinusoidal position command, depicted in Fig. 18 (a). The command starts at 0.2 s and it is initially smoothed multiplying it with a sigmoid function which vary from 0 to 1 between 0.2 s and 1 s. This simulation has been performed imposing the external force, the preload and the backlash equal to zero, therefore the force values are quite small since the only load is due to the inertia and the command has a low dynamic range. The only deviations between the speed trends happen in the speed inversion instants, highlighted in Fig. 17 with a boolean flag. When the speed is reversed, as can be seen in Fig. 18 (d), the normal contact forces cross the zero value (which in this model means that the contact angle sign is inverted). Therefore, there are not enough contact pressure anymore and the sphere slides for a short time, until the contact normal forces rise again to restart the motion in the other direction. Since the motion is imposed from the screw, the sliding occurs in the contact point B, as illustrated in Fig. 18 (d), looking at the right vertical axis: a value of 1 means that there is sliding, while a value of 0 indicates that there is no sliding. Obviously, having adopted a differentiable formulation for the tangential contact forces [70], there is always a little relative speed in the direction of rolling at the contact points: the boolean index of Fig. 17 and Fig. 18

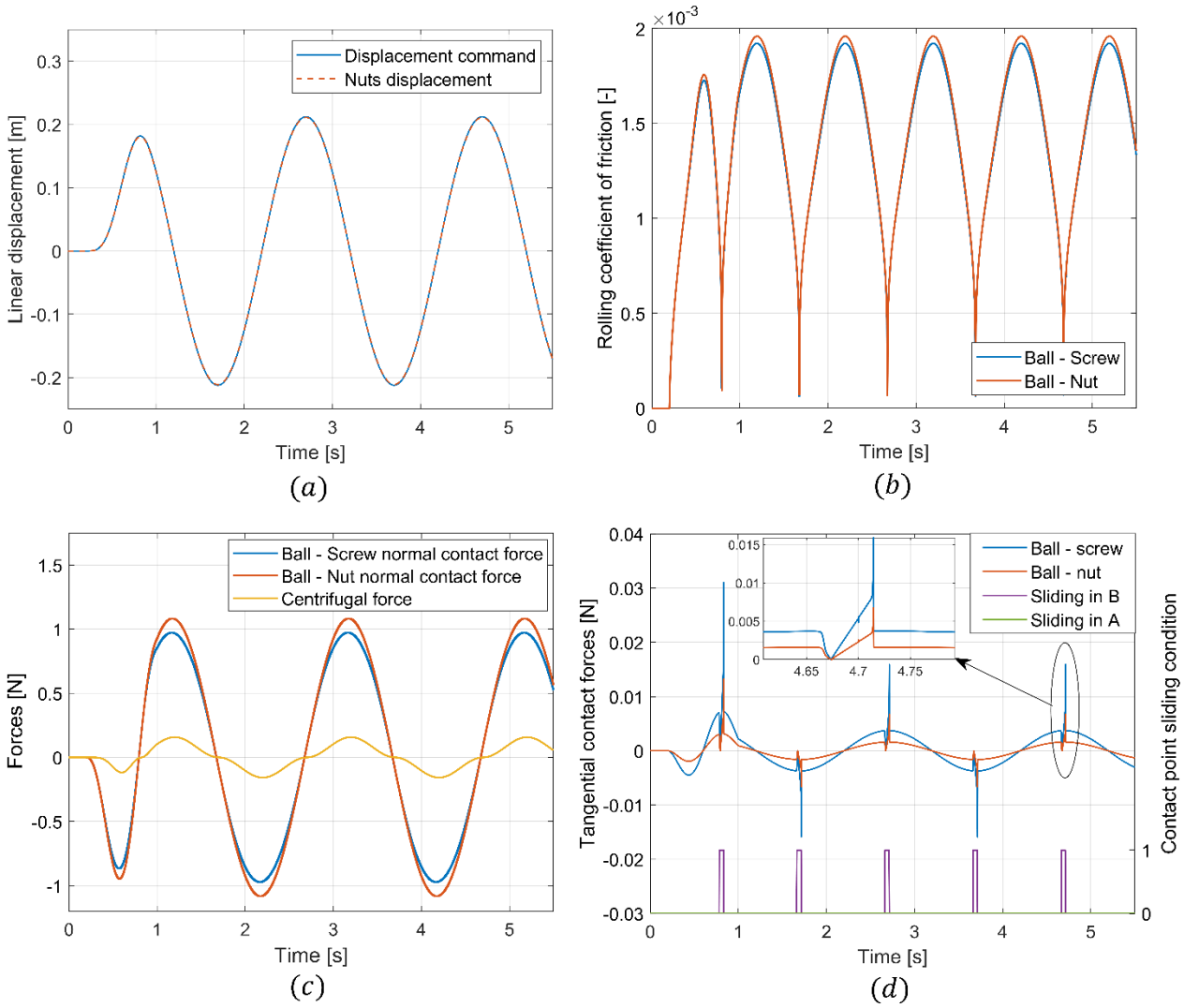

Fig. 18. Sinusoidal position command (a), rolling friction coefficient (b), centrifugal forces and contact normal forces (c) and tangential contact forces with boolean indicator for sliding conditions (d), for nut 1 ($j = 1$).

(d) is equal to 1 when this relative speed exceeds the threshold sliding speed corresponding to the peak of friction coefficient, beyond which the friction coefficient starts to decrease according to the stribeck effect to reach its dynamic value, while it is equal to 0 for lower relative speeds.

This transition reflects into the tangential contact forces, which goes first to zero when the normal forces are zero as well. In this moment the sphere starts to slide but when the normal contact forces rise again the adherence between sphere and screw groove is restored and the tangential forces exhibit a spike due to this transition. The difference between the values of the tangential contact forces in A and B derives from the difference between the normal contact forces, which is due to the centrifugal force (Fig. 18 (c)). As for the contact forces, the sign convention for the centrifugal force is the same: its sign is related the screw speed sign, but physically it is always oriented in the $-n$ axis direction. On the sphere acts the rolling friction force too, which is dependent on the normal forces and on the rolling friction coefficient. In Fig. 18 (b) it can be seen that also the rolling friction coefficient is affected by the centrifugal force effect, since it depends on normal contact forces, according to Eqns. (20-21). Therefore, the rolling friction torque is not a constant value but vary according to the variation of the other quantities.

A similar behaviour is obtained if a backlash of $0.05\ mm$ is injected in the two nuts, under the same simulation conditions and inputs, as shown in Fig. 19. During the normal movement the behaviour is the same of that without backlash of Fig. 18 (point 1): the sphere touches both the grooves with the motion imposed by the screw. When the speed inversion point is reached, due to the backlash, the components detach from each other and the contact forces drop to zero (point 2) and remain null until the backlash gap is closed again.

The sphere, which had an angular and linear speed along the helical path, continue to advance along the path and therefore the relative speed increases, since the screw is stopping. When the sphere enters again in contact with the other side of the screw groove, at first it starts to bounce a little between the grooves producing contact

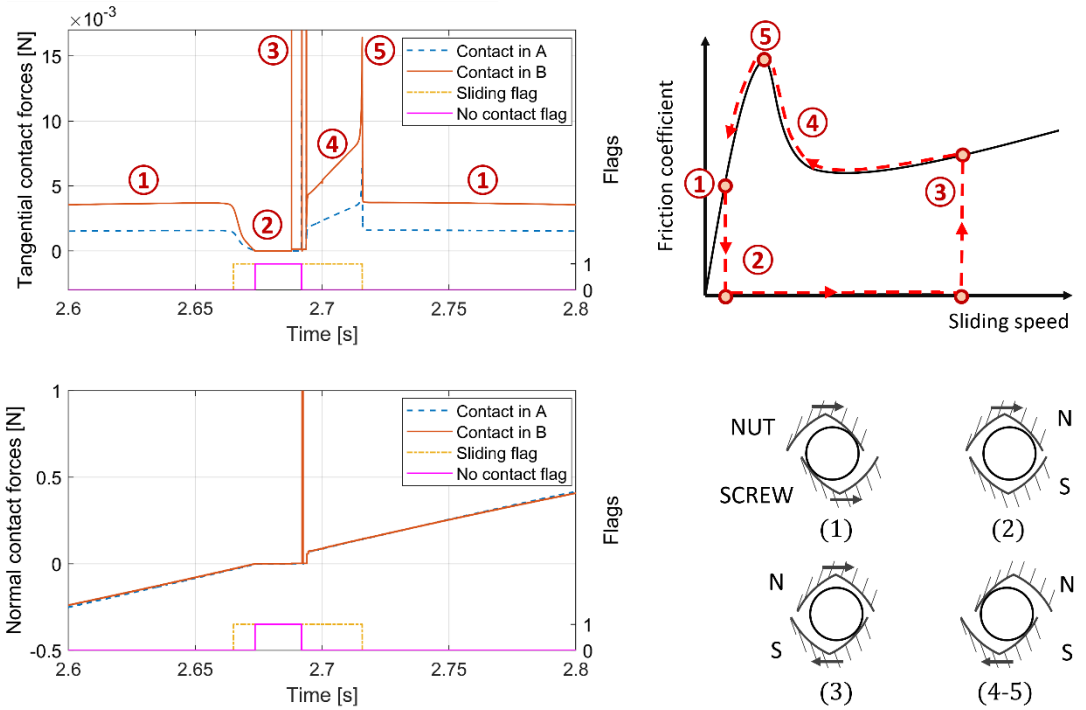

Fig. 19. Normal and tangential contact forces during a sphere's sliding event at speed inversion point, in presence of backlash.

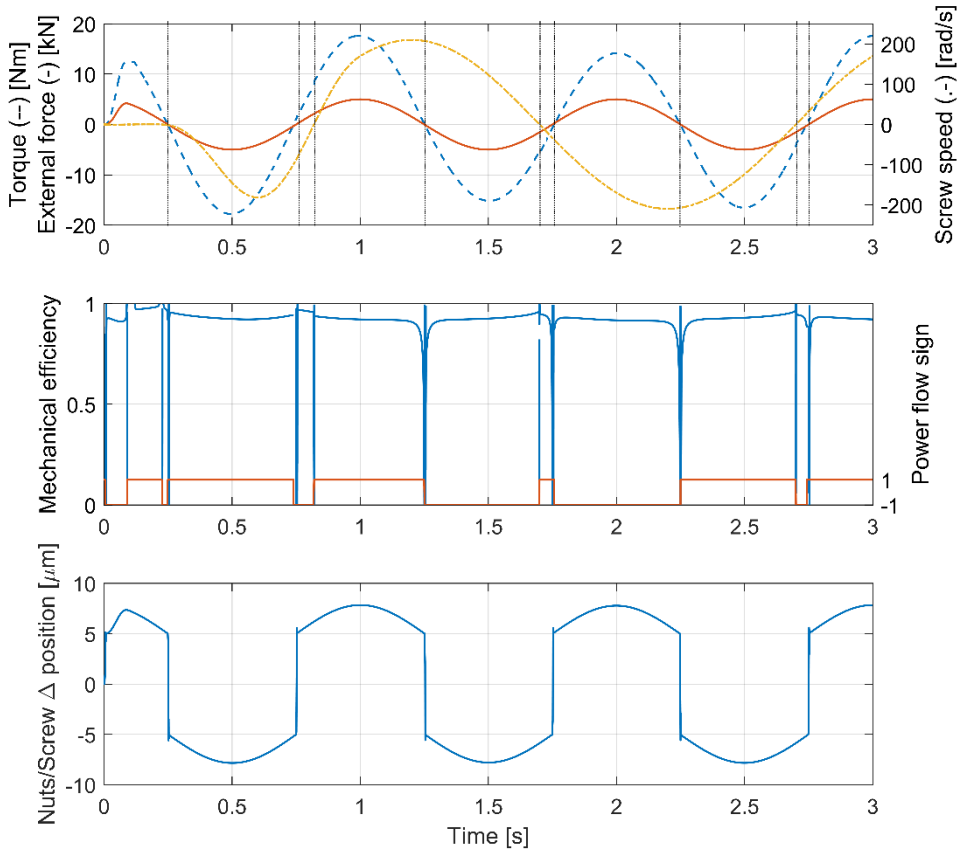

Fig. 20. Backlash and speed inversion effects on the mechanical efficiency in dynamics.

force peaks (point 3), until it remains blocked between the screw and the nut, which entered again in contact as well. At this point the normal contact forces are still low but not null: the sphere starts to slide, progressively decreasing the relative speed, until it goes below the threshold velocity, passing across the static friction peak force (point 5) and returning in an adherence condition (point 1). Fig. 19 shows a qualitative graph of these steps under the point of view of the friction coefficient.

Finally, Fig. 20 shows the effect of backlash and speed inversion on the mechanical efficiency in dynamic conditions. To highlight the backlash effect, the preload was set to zero while the backlash to $10\,\mu m$. A sinusoidal speed command was imposed with $200\,rad/s$ amplitude and a frequency of $0.5\,Hz$. A $1\,Hz$ sinusoidal external force was applied with amplitude of $5\,kN$. As a result, also the necessary torque shows the same frequency, superposed to that of command which can be noted looking at the torque amplitude. The mechanical efficiency presents a drop toward zero each time that either the speed change sign or the external force direction is reversed: these points are identified in the first subplot by the vertical dotted lines and the power flow sign, which is 1 when the screw speed is coherent with the applied torque, -1 otherwise. In the first situations, the ratio between output and input power of Eq. (22) assumes singular values and the efficiency shows abrupt changes. In the latter scenario, the external force inversion causes the sphere to change contact orientation, as can be seen from the third subplot of Fig. 20. Since backlash is present, for a short time the backlash gap opens and no force is transmitted, and the mechanical efficiency drops. The position difference between the nuts and the screw shows that as the external force rises the deformation in the contact areas increases, accordingly to previously simulations.
This level of detail at the sphere level cannot be reached through the commonly used equivalent perfect ACME screw model jointed with an elastic backlash and friction, such as those used in [69,76], and this is the reason why this approach is more useful and precise to describe the physics within the mechanism and it will be useful in the future analysis to support the model-based health monitoring.

5. Conclusions and Future Work

This paper presented a high-fidelity model of the rotary to linear conversion ball screw. It contributes to better understand the relation between preload and efficiency and it introduces into a dynamic model aspects which generally are not considered in literature, such as the backlash hysteresis, friction trends, transitions at speed inversion and double contact point sliding of balls in dynamics. It constitutes an advance with respect to the state of the art as it allows to obtain accurate results both in static and dynamic conditions considering only lumped parameter equations. This involves that the computational cost and the simulation time are much lower than those of multibody or 3D FEM models with a similar accuracy. The strong reduction in simulation time makes it a powerful tool to improve prognostic algorithms' effectiveness on EMAs since the model can be used as a virtual test rig, allowing to analyse a large number of operative conditions considering several possible defects, establishing the basis for detailed and accurate simulations of this mechanical component under healthy and degraded states.
The use of a fast model allows to study the influence of single or combined defects on the global performance and how various type of faults can evolve in time and cause macroscopic effects that can be detected by data analysis. The final goal is to capture a set of possible synthetic signals-based features that could be used to detect the flaw state, to monitor the component health status and then to infer the residual useful life. The mechanical efficiency can be one of those indicators because it is representative of the performance degradation but, alone, it is not sufficient to discriminate which fault has occurred and is progressing. To achieve such results a large database of features obtained from several simulations with different degradation levels is required: the simulation speed is then a crucial factor for such identification.
In this work the model was used to analyse the effects of single and combined defects. First, the effect of single parameters on the mechanical direct efficiency was analysed. Later, the influence of different parameters on the mechanical direct efficiency was studied, with particular attention to the preload and external force interaction. The model is capable of handling double-sided backlash efficiently and to describe in detail friction trends and balls dynamics: these parameters' effect on the dynamic behaviour were investigated, analysing different possible operating conditions based on the ratio between external force and preload. Finally, the effect of the centrifugal force on the normal and friction forces was investigated and the ability of the model to capture the rolling-sliding conditions and transition between them in both contact points was shown with and without backlash, together with mechanical efficiency variations during transients.
Future work will develop the model to enhance its capability to accurately describe the kinematics and dynamics of the components within the ball screw. The intended enhancements include a more detailed description of the preload system and of the contact forces exchanged by the spheres. Further enhancements regard the insertion of gyroscopic effects and the modelling of the recirculating system.
Finally, experimental validation of this model is paramount to rely on its results and to use it in PHM systems. Therefore, an experimental bench for ball screw EMAs is being set up to validate the model results. The present model is also useful as a driver for its design, to have a preliminary idea of which dynamics can be reached and therefore which motor and sensors have to be installed.

No color images in the printed version Declarations of interest: none.

Acknowledgements

The research work presented in this paper was performed within the ASTIB project, which has received funding from the Clean Sky 2 Joint Undertaking under the European Union's Horizon 2020 research and innovation programme under grant agreement CSJU – GAM REG 2014-2015.

Notations

A	Contact point between the ball and the nut.
B	Contact point between the ball and the screw.
C_f	Friction torque on the screw.
C_m	Motor torque on the screw.
C_{rf}	Total friction torque on the screw.
C_V	Resultant force of all the spheres on the screw.
F_{ext}	External axial force on the nuts.
F_{fr}	Friction force on each nut.
F_{rf}	Sliding/Rolling force tangential to the helical direction.
F_{max}	Ball screw critical load
F_{pr}	Preload force.
$F_{pr_{ISO}}$	Preload force indicated in the normative reference.
F_V	Reaction force of one sphere on the screw shaft in the tangential direction.
F_Z	Component of the force exchanged between one sphere and the nut in the screw axial direction.
H_A	Friction tangential force in A.
H_B	Friction tangential force in B.
H_c	Backlash coefficient.
I_b	Rotational moment of inertia of a ball around its centroid.
I_s	Moment of inertia of the screw.
M_b	Ball mass.
M_n	Mass of each nut.
P	Normal force in A on one sphere.
P'	Normal force in B on one sphere.
Z_{tot}	Total number of spheres in the loaded turns.
Z	Number of effective loaded spheres.
b_{max}	Maximum allowed backlash in the z_i direction.
c	Contact damping coefficient.
g_l	Sliding friction function of the sphere. ($l = 1, \dots 6$)
f_v	Rolling friction coefficient in A.
$f_v{}'$	Rolling friction coefficient in B.
f_{v0}	Rolling friction coefficient in A independent from the sphere angular speed.
f'_{v0}	Rolling friction coefficient in B independent from the sphere angular speed.
f_{v1}	Coefficient of rolling friction dependency from the sphere angular speed.
k	Contact stiffness.
k_{ax}	Ball screw axial stiffness.
k_{gc}	Coefficient of rolling friction dependency from the normal load in the contact points.
k_{rf}	Coefficient used in the sensitivity analysis to vary the rolling friction value.
n_t	Number of loaded turns of each nut.
p	Screw lead.
r_b	Ball radius.
r_m	Nominal screw radius.
u	Rolling friction parameter in A.
u'	Rolling friction parameter in B.
v_s	Sliding speed in the contact points.
y_b	Displacement of the ball along the linearized helical direction.

y_{up}	Displacement of the screw groove along the linearized helical direction.
z	Average linear displacement of the nuts in the axial direction.
z_b	Ball displacement on the direction normal to the contact plane.
z_n	Nut displacement on the direction normal to the contact plane.
z_s	Screw displacement on the direction normal to the contact plane.
α	Screw's nominal helix angle.
α'	Screw's helix angle in B.
α''	Screw's helix angles in A.
β, β_A, β_B	Contact angles.
Ω	Screw angular rotation.
Ω_{cr}	Ball screw critical angular speed for transverse vibration.
ω_{rev}	Sphere revolution speed around the screw axis.
η	Mechanical direct efficiency.
η_{th}	Theoretical mechanical direct efficiency.
ϑ_b	Angular rotation of a sphere around his x_i axis.
$()_i$	Contact point index ($i = A, B$).
$()_j$	Number of nut index ($j = 1, 2$).
$()_1$	Index for referring to the nut 1.
$()_2$	Index for referring to the nut 2.

References

[1] T. Ford, More-electric aircraft, Aircr. Eng. Aerosp. Technol. 77 (2005).

[2] S. Hesse, G. Konrad, R. Reichel, I. Schäfer, P. Bourlier, M. Buff, An Electro - Mechanical Actuator for General Aviation Aircraft, in: Aerosp. Technol. Conf. Expo., SAE, 2007: p. 11. doi:10.4271/2007-01-3900.

[3] J.-C. Maré, J. Fu, Review on signal-by-wire and power-by-wire actuation for more electric aircraft, Chinese J. Aeronaut. 30 (2017) 857–870. doi:10.1016/j.cja.2017.03.013.

[4] S.C. Jensen, G.D. Jenney, D. Dawson, Flight test experience with an electromechanical actuator on the F-18 Systems Research Aircraft, 19th Digit. Avion. Syst. 1 (2000) 1–11. doi:10.1109/DASC.2000.886914.

[5] J.-C. Derrien, P. Tieys, D. Senegas, M. Todeschi, EMA Aileron COVADIS Development, in: Aerosp. Technol. Conf. Expo., SAE, 2011: p. 13. doi:10.4271/2011-01-2729.

[6] M.J. Roemer, L. Tang, Integrated Vehicle Health and Fault Contingency Management for UAVs, in: Handb. Unmanned Aer. Veh., Springer Netherlands, Dordrecht, 2015: pp. 999–1025. doi:10.1007/978-90-481-9707-1_46.

[7] D.E. Blanding, A.J. Watanabe, Fault-tolerant electro-mechanical actuator having motor armatures to drive a ram and having an armature release mechanism, US 7,190,096 B2, 2007.

[8] J.W. Bennett, B.C. Mecrow, D.J. Atkinson, G.J. Atkinson, Safety-critical design of electromechanical actuation systems in commercial aircraft, IET Electr. Power Appl. 5 (2011) 37. doi:10.1049/iet-epa.2009.0304.

[9] L.L. V. Larson, R.K. Larsen, Fault-tolerant linear electromechanical actuator, 5,214,972, 1993.

[10] D. Tesar, Fault tolerant linear actuator, US 6,791,215 B2, 2004.

[11] D.H. Grimm, T.L. Jones, Jam tolerant linear actuator, 5,144,851, 1992.

[12] D.T. Nguyen, B.W. Behar, T.A. McKay, Jam-tolerant electromechanical actuator, US 8,794,084 B2, 2014.

[13] A.J. Collins, Flight control surface actuation system, US 6,776,376 B2, 2004. doi:10.1016/S0141.

[14] M. Todeschi, Airbus - EMAs for Flight Controls Actuation System - An Important Step Achieved in 2011, in: SAE Int., 2011. doi:10.4271/2011-01-2732.

[15] Y.M. Hussain, S. Burrow, L. Henson, P. Keogh, A Review of Techniques to Mitigate Jamming in Electromechanical Actuators for Safety Critical Applications, Int. J. Progn. Heal. Manag. (2018) 2153–2648.

[16] M. Todeschi, L. Baxerres, Health monitoring for the flight control EMAs, in: IFAC-PapersOnLine, Elsevier B.V., 2015: pp. 186–193. doi:10.1016/j.ifacol.2015.09.526.

[17] A. De Martin, G. Jacazio, G. Vachtsevanos, Anomaly Detection and Prognosis for Primary Flight Control EMAs, in: Eur. Conf. Progn. Heal. Manag. Soc., 2016: pp. 1–9.

[18] G. Vachtsevanos, F. Lewis, M. Roemer, A. Hess, B. Wu, Intelligent Fault Diagnosis and Prognosis for

Engineering Systems, John Wiley & Sons, Inc., Hoboken, NJ, USA, 2006. doi:10.1002/9780470117842.
[19] S. Nandi, H.A. Toliyat, X. Li, Condition monitoring and fault diagnosis of electrical motors - A review, IEEE Trans. Energy Convers. 20 (2005) 719–729. doi:10.1109/TEC.2005.847955.
[20] A. De Martin, G. Jacazio, G. Vachtsevanos, Windings Fault Detection and Prognosis in Electro-Mechanical Flight Control Actuators Operating in Active-Active Configuration, Int. J. Progn. Heal. Manag. (2017) 0–13.
[21] D.W. Brown, G. Georgoulas, B.M. Bole, Prognostics Enhanced Reconfigurable Control of Electro-Mechanical Actuators, in: Annu. Conf. Progn. Heal. Manag. Soc., 2009: pp. 1–17.
[22] D. Belmonte, M.D.L. Dalla Vedova, P. Maggiore, New Prognostic Method Based on Spectral Analysis Techniques Dealing with Motor Static Eccentricity for Aerospace Electromechanical Actuators, WSEAS Trans. Syst. (2015) 45–53.
[23] D. Brown, M. Abbas, A. Ginart, I. Ali, P. Kalgren, G. Vachtsevanos, Turn-off Time as a Precursor for Gate Bipolar Transistor Latch-up Faults in Electric Motor Drives, in: Annu. Conf. Progn. Heal. Manag. Soc., 2010: pp. 1–8.
[24] H. Li, X. Ye, C. Chen, G. Vachtsevanos, A framework for model-based diagnostics and prognostics of switched-mode power supplies, in: Proc. Annu. Conf. Progn. Heal. Manag. Soc. 2014, 2014: pp. 705–712.
[25] E. Balaban, A. Saxena, K. Goebel, Experimental data collection and modeling for nominal and fault conditions on electro-mechanical actuators, in: Annu. Conf. Progn. Heal. Manag. Soc., 2009: pp. 1–15.
[26] E. Balaban, A. Saxena, S. Narasimhan, I. Roychoudhury, K.F. Goebel, M.T. Koopmans, Airborne electro-mechanical actuator test stand for development of prognostic health management systems, in: Annu. Conf. Progn. Heal. Manag. Soc., 2010: pp. 1–13.
[27] C. Lessmeier, O. Enge-Rosenblatt, C. Bayer, D. Zimmer, Data Acquisition and Signal Analysis from Measured Motor Currents for Defect Detection in Electromechanical Drive Systems, in: Eur. Conf. Progn. Heal. Manag. Soc. 2014, 2014: pp. 1–10. doi:10.13140/2.1.3499.3289.
[28] S. Mauro, S. Pastorelli, T. Mohtar, Sensitivity Analysis of the Transmission Chain of a Horizontal Machining Tool Axis to Design and Control Parameters, Adv. Mech. Eng. 6 (2014) 169064. doi:10.1155/2014/169064.
[29] S. Mauro, S. Pastorelli, E. Johnston, Influence of controller parameters on the life of ball screw feed drives, Adv. Mech. Eng. 7 (2015) 1–11. doi:10.1177/1687814015599728.
[30] R. Bertolaso, M. Cheikh, Y. Barranger, J.-C. Dupré, A. Germaneau, P. Doumalin, Experimental and numerical study of the load distribution in a ball-screw system, J. Mech. Sci. Technol. 28 (2014) 1411–1420. doi:10.1007/s12206-014-0128-0.
[31] C.J. Chen, W. Jywe, Y.C. Liu, H.H. Jwo, The development of using the digital projection method to measure the contact angle of ball screw, Phys. Procedia. 19 (2011) 36–42. doi:10.1016/j.phpro.2011.06.122.
[32] G.A. Levit, Recirculating ball screw and nut units, Mach. Tool. 34 (1963) 3–8.
[33] G.A. Levit, Calculations of recirculating ball screw and nut transmission, Mach. Tool. 5 (1963) 9–16.
[34] C.C. Wei, J.F. Lin, Kinematic Analysis of the Ball Screw Mechanism Considering Variable Contact Angles and Elastic Deformations, J. Mech. Des. 125 (2003) 717–733. doi:10.1115/1.1623761.
[35] M.C. Lin, S.A. Velinsky, B. Ravani, Design of the Ball Screw Mechanism for Optimal Efficiency, J. Mech. Des. 116 (1994) 856–861.
[36] C.C. Wei, J.F. Lin, J.-H. Horng, Analysis of a ball screw with a preload and lubrication, Tribol. Int. 42 (2009) 1816–1831. doi:10.1016/j.triboint.2008.12.013.
[37] C.C. Wei, R.S. Lai, Kinematical analyses and transmission efficiency of a preloaded ball screw operating at high rotational speeds, Mech. Mach. Theory. 46 (2011) 880–898. doi:10.1016/j.mechmachtheory.2011.02.009.
[38] M.C. Lin, B. Ravani, S.A. Velinsky, Kinematics of the Ball Screw Mechanism, J. Mech. Des. 116 (1994) 849–855.
[39] Y.N. Drozdov, Calculating the wear of a screw and nut transmission with sliding friction, Sov. Eng. Res. 4 (1984) 1–12.
[40] H.-T.T. Huang, B. Ravani, Contact Stress Analysis in Ball Screw Mechanism Using the Tubular Medial Axis Representation of Contacting Surfaces, J. Mech. Des. 119 (1997) 8. doi:10.1115/1.2828794.
[41] R. Gnanamoorthy, N. Govindarajan, Y. Mutoh, Effect of slid-roll ratio on the contact fatigue behavior of sintered and hardened steels, J. Fail. Anal. Prev. 4 (2004) 78–83. doi:10.1361/15477020419082.

[42] N. Govindarajan, R. Gnanamoorthy, Rolling/sliding contact fatigue life prediction of sintered and hardened steels, Wear. 262 (2007) 70–78. doi:10.1016/j.wear.2006.03.053.
[43] J. Hu, M. Wang, T. Zan, The kinematics of ball-screw mechanisms via the slide-roll ratio, Mech. Mach. Theory. 79 (2014) 158–172. doi:10.1016/j.mechmachtheory.2014.04.017.
[44] J.F. Cuttino, T.A. Dow, Contact Between Elastic Bodies With an Elliptic Contact Interface in Torsion, J. Mech. Des. 64 (1997) 144–148. doi:10.1115/1.2788970.
[45] J.F. Cuttino, T.A. Dow, B.F. Knight, Analytical and Experimental Identification of Nonlinearities in a Single-Nut, Preloaded Ball Screw, J. Mech. Des. 119 (1997) 15. doi:10.1115/1.2828782.
[46] C.E. Okwudire, Improved Screw–Nut Interface Model for High-Performance Ball Screw Drives, J. Mech. Des. 133 (2011) 041009. doi:10.1115/1.4004000.
[47] M.F. Zaeh, T. Oertli, J. Milberg, Finite Element Modelling of Ball Screw Feed Drive Systems, CIRP Ann. - Manuf. Technol. 53 (2004) 289–292. doi:10.1016/S0007-8506(07)60700-8.
[48] C.E. Okwudire, Y. Altintas, Hybrid Modeling of Ball Screw Drives With Coupled Axial, Torsional, and Lateral Dynamics, J. Mech. Des. 131 (2009) 071002. doi:10.1115/1.3125887.
[49] B. Lin, C.E. Okwudire, J.S. Wou, Low Order Static Load Distribution Model for Ball Screw Mechanisms including Effects of Lateral Deformation and Geometric Errors, J. Mech. Des. 140 (2018) 1–12. doi:10.1115/1.4038071.
[50] B. Lin, C.E. Okwudire, Low-Order Contact Load Distribution Model for Ball Nut Assemblies, SAE Int. J. Passeng. Cars - Mech. Syst. 9 (2016) 2016-01-1560. doi:10.4271/2016-01-1560.
[51] G.H. Feng, Y.L. Pan, Investigation of ball screw preload variation based on dynamic modeling of a preload adjustable feed-drive system and spectrum analysis of ball-nuts sensed vibration signals, Int. J. Mach. Tools Manuf. 52 (2012) 85–96. doi:10.1016/j.ijmachtools.2011.09.008.
[52] G.H. Feng, Y.L. Pan, Establishing a cost-effective sensing system and signal processing method to diagnose preload levels of ball screws, Mech. Syst. Signal Process. 28 (2012) 78–88. doi:10.1016/j.ymssp.2011.10.004.
[53] P. Li, X. Jia, J. Feng, H. Davari, G. Qiao, Y. Hwang, J. Lee, Prognosability study of ball screw degradation using systematic methodology, Mech. Syst. Signal Process. 109 (2018) 45–57. doi:10.1016/j.ymssp.2018.02.046.
[54] A. Isturiz, J. Vinals, J.M. Abete, A. Iturrospe, Health monitoring strategy for electromechanical actuator systems and components. Screw backlash and fatigue estimation, in: Recent Adv. Aerosp. Actuation Syst. Components, 2012.
[55] E. Balaban, A. Saxena, P. Bansal, K.F. Goebel, P. Stoelting, S. Curran, A diagnostic approach for electro-mechanical actuators in aerospace systems, in: IEEEAC, 2009: p. 1345.
[56] J.P. Hung, J. Shih-Shyn Wu, J.Y. Chiu, Impact failure analysis of re-circulating mechanism in ball screw, Eng. Fail. Anal. 11 (2004) 561–573. doi:10.1016/j.engfailanal.2004.01.002.
[57] W. Jin, Y. Chen, J. Lee, Methodology for Ball Screw Component Health Assessment and Failure Analysis, Vol. 2 Syst. Micro Nano Technol. Sustain. Manuf. (2013) V002T02A031. doi:10.1115/MSEC2013-1252.
[58] T.E. Tallian, On competing failure modes in rolling contact, ASLE Trans. 10 (1967) 418–439. doi:10.1080/05698196708972201.
[59] A.C. Bertolino, G. Jacazio, S. Mauro, M. Sorli, High Fidelity Model of a Ball Screw Drive for a Flight Control Servoactuator, in: ASME (Ed.), IMECE, ASME, Tampa, Florida, USA, 2017: p. V001T03A024. doi:10.1115/IMECE2017-70737.
[60] A.C. Bertolino, G. Jacazio, S. Mauro, M. Sorli, High fidelity model for efficiency calculation of ball screws for flight control actuators, in: Recent Adv. Aerosp. Actuation Syst. Components, Tolouse, France, 2018: pp. 153–163.
[61] R.W. Pratt, Flight control systems: practical issues in design and implementation, Roger W. Pratt, 2000.
[62] S. Wang, M. Tomovic, H. Liu, Aircraft Hydraulic Systems, in: Elsevier (Ed.), Commer. Aircr. Hydraul. Syst., Elsevier, 2016: pp. 53–114. doi:10.1016/B978-0-12-419972-9.00002-4.
[63] R.P. Elbert, M.A. Hafner, Fault tolerant actuation system for flight control actuators, 5806805, 1998.
[64] L. Wang, J.-C. Maré, Y. Fu, Investigation in the Dynamic Force Equalization of Dissimilar Redundant Redundant Actuation Systems Operating in Active/Active Mode, in: 28Th Int. Congr. Aeronaut. Sci., 2012.
[65] G. Balbo, R. Graziosi, Viti a ricircolazione di sfere: risultato del contratto di ricerca con oggetto: analisi sperimentale di sitemi a ricircolazione di sfere, per mezzo di un apposito banco di misura - Parte prima, Collana di, Consiglio nazionale delle ricerche - Programma di ricerca sull'automazione nell'industria

meccanica con speciale riguardo alle macchine utensili, Milano, 1970.
[66] S. Andersson, A. Söderberg, S. Björklund, Friction models for sliding dry, boundary and mixed lubricated contacts, Tribol. Int. 40 (2007) 580–587. doi:10.1016/j.triboint.2005.11.014.
[67] Y. Chen, W. Tang, Dynamic contact stiffness analysis of a double-nut ball screw based on a quasi-static method, Mech. Mach. Theory. 73 (2014) 76–90. doi:10.1016/j.mechmachtheory.2013.10.008.
[68] M. Nordin, J. Galic', P.-O. Gutman, New models for backlash and gear play, Int. J. Adapt. Control Signal Process. 11 (1997) 49–63. doi:10.1002/(SICI)1099-1115(199702)11:1<49::AID-ACS394>3.0.CO;2-X.
[69] J.-C. Maré, Requirement-based system-level simulation of mechanical transmissions with special consideration of friction, backlash and preload, Simul. Model. Pract. Theory. 63 (2016) 58–82. doi:10.1016/j.simpat.2016.01.005.
[70] C. Makkar, W.E. Dixon, W.G. Sawyer, G. Hu, A New Continuously Differentiable Friction Model for Control Systems Design, in: Int. Conf. Adv. Intell. Mechatronics, IEEE/ASME, Monterey, California, 2005: pp. 600–605.
[71] G. Jacazio, B. Piombo, Meccanica applicata alle macchine - Vol. I, Levrotto & Bella, Torino, 1991.
[72] G. Straffelini, Friction and Wear, Springer International Publishing, Cham, 2015. doi:10.1007/978-3-319-05894-8.
[73] ISO 3408-4:2006, Ball screws - Part 4: Static axial rigidity, (2006).
[74] P.C. Tsai, C.C. Cheng, Y.C. Hwang, Ball screw preload loss detection using ball pass frequency, Mech. Syst. Signal Process. 48 (2014) 77–91. doi:10.1016/j.ymssp.2014.02.017.
[75] T.L. Nguyen, S.K. Ro, C.K. Song, J.K. Park, Study on preload monitoring of ball screw feed drive system using natural frequency detection, J. Korean Soc. Precis. Eng. 35 (2018) 135–143. doi:10.7736/KSPE.2018.35.2.135.
[76] J. Fu, J.-C. Maré, Y. Fu, Modelling and simulation of flight control electromechanical actuators with special focus on model architecting, multidisciplinary effects and power flows, Chinese J. Aeronaut. 30 (2017) 47–65. doi:10.1016/j.cja.2016.07.006.